CrossMark

R E V I E W

Metal Nanoparticles in Ionic Liquids

Susann Wegner[1] · Christoph Janiak[1]

Abstract During the last years ionic liquids (ILs) were increasingly used and investigated as reaction media, hydrogen sources, catalysts, templating agents and stabilizers for the synthesis of (monometallic and bimetallic) metal nanoparticles (M-NPs). Especially ILs with 1,3-dialkyl-imidazolium cations featured prominently in the formation and stabilization of M-NPs. This chapter summarizes studies which focused on the interdependencies of the IL with the metal nanoparticle and tried to elucidate, for example, influences of the IL-cation, -anion and alkyl chain length. Qualitatively, the size of M-NPs was found to increase with the size of the IL-anion. The influence of the size of imidazolium-cation is less clear. The M-NP size was both found to increase and to decrease with increasing chain lengths of the 1,3-dialkyl-imidazolium cation. It is evident from such reports on cation and anion effects of ILs that the interaction between an IL and a (growing) metal nanoparticle is far from understood. Factors like IL-viscosity, hydrogen-bonding capability and the relative ratio of polar and non-polar domains of ILs may also influence the stability of nanoparticles in ionic liquids and an improved understanding of the IL-nanoparticle interaction would be needed for a more rational design of nanomaterials in ILs. Furthermore, thiol-, ether-, carboxylic acid-, amino- and hydroxyl-functionalized ILs add to the complexity by acting also as coordinating capping ligands. In addition imidazolium cations are precursors to *N*-heterocyclic carbenes, NHCs which form from imidazolium-based ionic liquids by in situ deprotonation at the acidic C2-H ring position as intermediate species during the nanoparticle

---

✉ Christoph Janiak
janiak@uni-duesseldorf.de

[1] Institut für Anorganische Chemie und Strukturchemie, Heinrich-Heine Universität Düsseldorf, Universitätsstr. 1, 40225 Düsseldorf, Germany

🙋 Springer

seeding and growth process or as surface coordinating ligand for the stabilization of the metal nanoparticle.

Keywords Ionic liquids · Metal nanoparticles · Cation and anion effects · Alkyl chain effects · Stabilization

1 Introduction

Already in the nineteenth century the first research efforts were seen on the synthesis of nanoparticles and the study of their properties [1–6]. Michael Faraday found in 1857 that nano-alloys can be synthesized by chemical reduction of noble-metal compounds and placed solutions of metal salt precursors with Au, Pt and Ag in a reducing atmosphere of "sulphured hydrogen" [7]. Over the last decades the evolvement of imaging methods like electron and scanning microscopies together with the application oriented interest in their properties has led to an exponential growth of metal nanoparticle (M-NP) research [8–10]. M-NPs have become significant for applications in medicine [11, 12], optics [13, 14], electronics [15], luminescence [16] and catalysis [17–19].

The synthesis of metal nanoparticles can be commonly carried out by chemical reduction [20–22], electrochemical reduction [23] and thermal decomposition [24] also induced by microwave heating [25–27]. Through the synthetic methodology, it is possible to vary the morphology, size and size distribution of M-NPs. Strong reducing agents such as sodium hydride seldom control the size and shape of M-NPs but mild reducing agents such as sodium citrate and ascorbic acid [28] which simultaneously act as coordinating capping ligands can control the size and shape of metal NPs. The size of metal nanoparticles could also be controlled by varying the concentration of metal salt precursors, reducing agents, pH, and temperature [28].

Depending on the application, e.g., in catalysis a small nanoparticle size of for example less than 5 nm may be desirable. At the same time, agglomeration of such small nanoparticles in the process of Ostwald-ripening needs to be avoided (Fig. 1).

To avoid agglomeration the nanoparticles have to be stabilized sterically or electrostatically (see also Sect. 4). For this, M-NPs are typically surrounded by coordinating (capping) ligands, by surfactants (electrostatic stabilization) or organic polymers (steric stabilization) (Fig. 2) [30]. Examples for common capping ligands are thiols, organic acids, alcohols or amines. Protic ligands like thiols and organic acids become deprotonated upon surface coordination and bind to the surface metal atoms as thiolates and carboxylates. In turn, the metal surface layer can be assumed to become cationic [31, 32]. The mean size of dodecanethiolate-stabilized Au nanoclusters can be finely adjusted by the Au:dodecanethiolate ratio and the temperature and rate at which the reduction is conducted to vary between diameters of 1.5 and 5.2 nm ($\sim$110–4800 Au atoms/core) [31]. Phosphine-stabilized gold nanoparticles can be easily prepared from $HAuCl_4$ trihydrate and sodium borohydride in the presence of triphenylphosphine in a water/toluene mixture where tetraoctylammonium bromide transferred the reactants into the organic phase. The biphasic synthesis can be carried out quickly under ambient conditions, permits
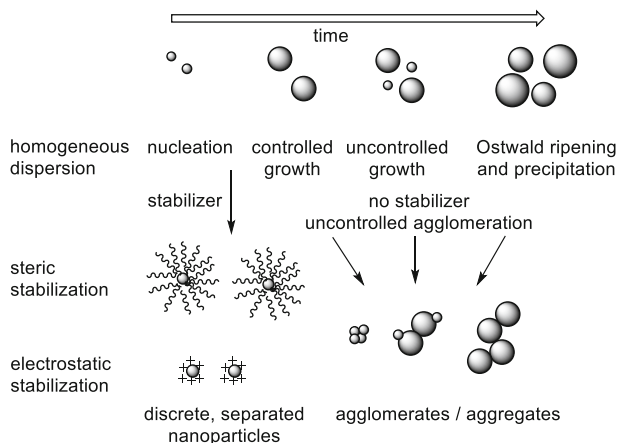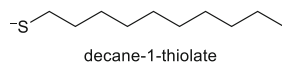
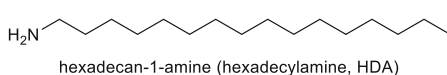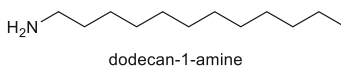**Fig. 1** Schematic presentation of (metal) nanoparticle growth and stabilization [29]
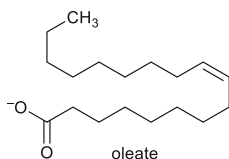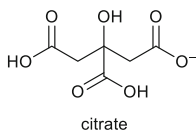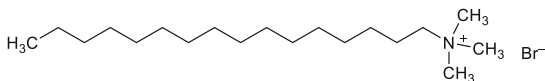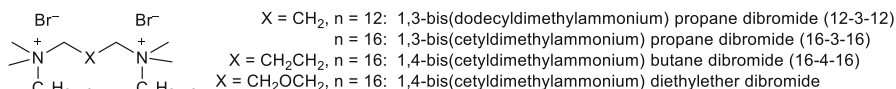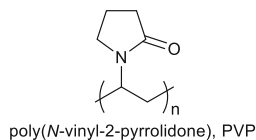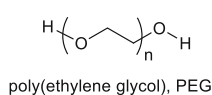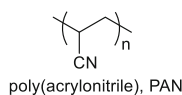
Fig. 2 Examples of typical classic stabilizers for metal nanoparticles

the use of a variety of phosphines as passivating ligands, and provides control over particle core size to produce 1.5-nm nanoparticles [33]. Phosphine-stabilized nanoparticles are precursors to other functionalized nanoparticle building blocks where nearly any functional group can be introduced into the ligand shell, and the metal core size can be tuned from 1.4 to 10 nm in diameter through ligand exchange reactions [34]. Further, non-agglomerated Ru- and Pt-NPs with a diameter of 2 ± 1 nm were prepared in ethylene glycol with acetate as coordination and stabilizing ligand [35], small Ru-NPs with a diameter of 2–3 nm were stabilized with alkylamines and alkylthiols [36].

Examples for surfactants used in the stabilization of metal nanoparticles are sodium dodecylsulfate (SDS) for Pd-NPs [37], gemini surfactants (cf. Figure 2) for Au-NPs, Ag-NPs, Au/Ag-alloy-NPs, Pd-NPs and Pt-NPs [38–42] or cetyltrimethylammonium bromide (CTAB) [42].

Examples for stabilizing polymers (cf. Figure 2) are poly(ethylene glycol), poly(acrylonitrile) and poly(vinylpyrrolidone). Poly(ethylene glycol) (PEG) can be used to control the formation and stability of Ag-NPs [43]. With poly(acrylonitrile) (PAN) it is possible to stabilize Pd-NPs with a nanoparticle diameter of 10–60 nm [44] and poly(vinylpyrrolidone) (PVP) can be used as stabilizer for Ag-NP in hybrid latex mini-emulsion at higher temperatures above 150 °C [45]. Gold and silver nanoparticles can be prepared from $HAuCl_4$ and $AgNO_3$, respectively, by using polysaccharides as reducing/stabilizing agents to obtain positively charged chitosan-stabilized gold nanoparticles and negatively charged heparin-stabilized silver nanoparticles inside the nanoscopic polysaccharide templates. The morphology and size distribution of prepared gold and silver nanoparticles varied with the concentration of both the polysaccharides and the precursor metal salts [46].

At the same time, the stabilization of M-NPs by the aforementioned coordinating capping ligands, surfactants or polymers results in a change of the surface properties and the surface accessibility of the nanoparticles particularly with regard to applications in catalysis [47].

2 Ionic Liquids

An alternative way for stabilizing metal nanoparticles can be the use of ionic liquids (ILs). By definition ionic liquids are molten organic or inorganic salts with a melting point below 100 °C [48–51], for practical purposes ILs are preferably already liquid at room temperature (RTILs). The low melting point of the ionic liquids is due to their low lattice energy, which in turn is a consequence of having weakly coordinating cations and anions. The weakly coordinating ion character derives from having large and mostly only single-charged ions so that the charge is delocalized over a large surface area. Consequently, the Coulomb attraction between ions with an effectively low surface charge density is weak. Examples of typical non-functionalized IL cations and anions are shown in Fig. 3. ILs have a very low vapor pressure which makes them easy to handle solvents [52], albeit problematic to recycle and purify by distillation. The thermal stability of typical ILs usually extends to 200 °C and even above [53–57]. Further, their physical properties

Weakly coordinating cations:
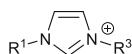
[R^{1}R^{3}Im]$^+$, 1-alkyl-3-alkyl-imidazolium,
e.g. [C$_4$C$_1$Im]$^+$: 1-n-butyl-3-methyl-imidazolium
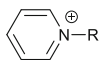
N-alkyl-pyridinium,
e.g. [C$_4$Py]$^+$: N-n-butyl-
pyridinium
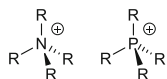
tetra-alkyl-ammonium,
tetra-alkyl-phosphonium,
e.g. [N$_{4111}$]$^+$: n-butyl-trimethyl-ammonium

Weakly coordinating anions (WCAs):

[BF$_4$]$^-$, tetrafluoroborate   [PF$_6$]$^-$, hexafluorophosphate

[CF$_3$SO$_3$]$^-$, [OTf]$^-$ trifluoromethanesulfonate (triflate)

[(CF$_3$SO$_2$)$_2$N]$^-$, [NTf$_2$]$^-$, bis(trifluoromethylsulfonyl)imide

[N(CN)$_2$]$^-$, dicyanamide

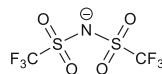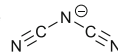[C(CN)$_3$]$^-$, tricyanomethanide
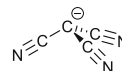
[B(CN)$_4$]$^-$, tetracyanoborate
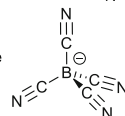
Fig. 3 Typical cations and anions of common non-functionalized ILs

like high polarity, high charge density and high dielectric constant [58] together with the formation of supramolecular mesoscopic networks [59] sets them apart from conventional organic solvents.

The well-established and probably most studied ILs contain an imidazolium cation (e.g. 1-ethyl-3-methylimidazolium [C$_2$C$_1$Im]$^+$ or 1-butyl-3-methylimida-zolium [C$_4$C$_1$Im]$^+$) [60] and weakly-coordinating anions (WCAs) such as tetrafluoroborate [BF$_4$]$^-$, hexafluorophosphate [PF$_6$]$^-$ and trifluoromethylsulfonate (triflate) [CF$_3$SO$_3$]$^-$ ([OTf]$^-$) or bis(trifluoromethylsulfonyl)imide (triflimide) [(CF$_3$SO$_2$)$_2$N]$^-$ ([NTf$_2$]$^-$) [61, 62]. ILs with the 1-n-butyl-3-methylimidazolium [C$_4$C$_1$Im]$^+$ cation and the relatively weakly coordinating anions tetrafluoroborate, hexafluorophosphate and trifluoromethanesulfonate, are liquids over a large range of temperatures (down to -80 °C), possess high thermal and chemical stability, a large electrochemical window, high ion density, relatively low viscosity, and negligible vapor pressure [63].

Variation of the side chain R, R^1, R^3 (cf. Figure 3) of the cation or variation of the anion results in a change of the physicochemical properties of the IL like thermal behavior, viscosity and density. The viscosity increases with the length of the side chain of the imidazolium cation from [C$_2$C$_1$Im][(CF$_3$SO$_2$)$_2$N] to [C$_8$C$_1$Im][(CF$_3$SO$_2$)$_2$N] whereas the ionic conductivity decreases [64].

3 Metal Nanoparticles in Ionic Liquids

In the last years many different M-NPs (monometallic and bimetallic) in ILs were obtained. The activities in this field have already been summarized in reviews which provide an overview of available metal nanoparticles in ionic liquids with their precursor, size and size dispersion. "A short review on stable metal nanoparticles using ionic liquids, supported ionic liquids and poly(ionic liquids)" focused on supported IL-like phases and on different types of poly(ionic liquids) [P(ILs)] and

polyelectrolytes as stabilizing agents for the synthesis of M-NPs. P(ILs) are an emerging class of cationic polymers with a poly(vinyl) backbone, e.g., from the polymerization of 1-vinyl-3-alkyl-imidazolium salts. P(ILs) possess properties of polymers as well as ILs with tunable properties through the anion and varying imidazolium alkyl chain length [8]. The main focus of the review "On the structural and surface properties of transition-metal nanoparticles in ionic liquids" [65] is on the different synthesis methods of transition-metal nanoparticles in ILs, the polar and non-polar regions in the M-NP/IL dispersion and steric and electronic protective layer formation against aggregation or agglomeration of the M-NPs. Further this review discusses the use of stable transition-metal NPs in ILs as green catalysts for several reactions and also as novel materials for chemical sensors. Particular attention is also paid to the stabilization models proposed to explain the stability and properties of the M-NP/IL dispersion [65]. The reviews entitled "naked metal nanoparticles from metal carbonyls in ionic liquids: Easy synthesis and stabilization" [47] and "synthesis and application of metal nanoparticle catalysts in ionic liquid media using metal carbonyl complexes as precursors" [66] *inter alia* summarize work on the synthesis of metal nanoparticles in ionic liquids from metal carbonyls. Commercially available binary metal carbonyls $M_x(CO)_y$ are unique precursors as they contain the metal atoms already in the zero-valent oxidation state needed for M-NPs. Thus, no reduction process is necessary and the only side-product CO is easily given off to the gas phase and removed from the reaction mixture. The microwave induced thermal decomposition of metal carbonyls in ILs provides an especially rapid and energy-saving procedure because of the ILs significant absorption efficiency for microwave energy. Examples for the direct use of M-NP/IL dispersions in hydrogenation catalysis of cyclohexene and benzene, Fischer–Tropsch reaction, and dehydration catalysis are also given in these reviews [47, 66]. The synthesis of metal nanoparticles from bulk metals, metal salts, metal complexes and metal carbonyls in ILs was reviewed in [30, 67, 68]. The synthesis of M-NPs in ILs can be carried out by chemical or electroreduction, thermolysis and photochemical methods including decomposition by microwave or sono-/ultrasound irradiation. Gas-phase syntheses can use sputtering, plasma/glow-discharge electrolysis and physical vapor deposition or electron beam and γ-irradiation. The in situ deposition of the M-NPs on supports, such as graphene-type materials was also addressed as was the use of M-NP/IL dispersions or on supports as catalysts for C–C coupling or hydrogenation catalysis [30, 67, 68]. The minireview "ionic liquids for the convenient synthesis of functional nanoparticles and other inorganic nanostructures" focusses on ionic liquids in the synthesis of crystalline nanoparticles at ambient temperatures and self-assembled, highly organized hybrid nanostructures [69].

The scope of this review here is the stabilization of metal nanoparticles in ionic liquids and the elucidation of the different factors which play a role in the stabilization and control the metal nanoparticle formation.

Briefly, metal nanoparticles of Rh, Pd, Pt, Ir, Fe, Ru, Co, Au, Ag, Cu and Ni were obtained from $RhCl_3 \cdot 3H_2O$, $PdCl_2$, $Pt_2(dba)_3$ (dba = dibenzylidene acetone), $[Ir(COD)Cl]_2$, $Fe_2(CO)_9$, $Ru(COD)(COT)$, $Co_2(CO)_8$, $KAuCl_4$, $AgBF_4$, $Cu(NO_3)_2$ and $Ni(COD)_2$. Metal nanoparticles have been synthesized mostly in the ionic

liquids $[C_4C_1Im][PF_6]$, $[C_4C_1Im][BF_4]$, $[C_4C_1Im][CF_3SO_3]$, $[C_{10}C_1Im][NTf_2]$, $[C_4C_1Im][NTf_2]$ by hydrogenation, chemical reduction and thermal decomposition. Sizes of M-NPs in ILs were found from 2.3 nm (Rh) [70], 4.2 ± 0.8 nm (Pd) [71], 2.8–3.3 nm (Pt) [116], 2–3 nm (Ir) [76], 5.2 nm (Fe) [72], 2.6 ± 0.4 nm (Ru) [73], 14 nm (Co) [164], 2.6-200 nm (Au) [74], 3–5 nm (Ag) [75], 3.5–9.5 nm (Cu) [76] and 5.1–5.9 nm for Ni [137]. Imidazolium ILs feature prominently in the formation and stabilization of M-NPs [77]. Imidazolium ILs are air, water and electrochemically stable with a wide liquidus range.

1-Alkyl-3-alkyl'-imidazolium ILs simultaneously act as reaction media, hydrogen sources, catalysts, templating agents and stabilizers for the synthesis of metal nanoparticles. It should be clear, however, that there are ILs which (i) have a strong influence on particle formation, (ii) which are good nucleation aids, but poor stabilizers, (iii) which are good nucleation aids and good stabilizers, and (iv) are none of this [78].

Examples of recent M-NP syntheses are given in Table 1. The examples show that metal nanoparticle synthesis occurs often by reduction of metal salts with added reducing agents such as H_2 or $NaBH_4$. Alternatively, the IL imidazolium cation with its protic C2-H or salt anions such as acetate, acetylacetonate, 1-(dimethylamino)propan-2-olate ($^-OCH(Me)CH_2NMe_2$) or amidinate ($MeC(N^iPr)_2^-$) act as internal or intramolecular reductants. The entries in Table 1 also show that microwave induced heating features prominently because of the very high absorption efficiency of ILs for microwave energy.

4 Stabilization of Metal Nanoparticles

Generally, the stabilization of M-NPs occurs through (I) electrostatic or (II) steric stabilization or (III) a combination of both electrostatic and steric stabilization [91]. The effect of stabilizing agents for nanoparticles is to build up a repulsive force between the particles [92], or at least to decrease any attractive van der Waals forces. Stabilizing agents surround NPs to prevent the agglomeration. The mechanism of stabilization has first been described in the Derjaguin–Landau–Verwey–Overbeek theory [93, 94].

4.1 Derjaguin-Landau-Verwey-Overbeek theory (DLVO theory)—Electrostatic Stabilization and Van Der Waals Interactions

The classic and most commonly used theory of a "mechanism of stabilization" was put forward by Derjaguin and Landau in 1940 as a quantitative theory [95] and later by Verwey and Overbeek in 1948 [96]. Both descriptions referred to colloidal materials. This basic theory combines repulsive Coulomb and attractive van der Waals (vdW) forces through the sum of an effective electrostatic term and a van der Waals term for the stabilization of these materials. Van der Waals forces originate from correlations between electron motions leading to non-spherical electron distributions in two adjacent particles or molecules. VdW forces are short-range, unidirectional and relatively weak compared to other intermolecular interactions.

Table 1 Recent mono and bimetallic NP synthesis in imidazolium ILs

Ionic liquid	Precursor	Conditions, reducing agent	NP with particle diameter	References
			Monometallic M-NPs	
$[C_4C_1Im][PF_6]$	$RhCl_3 \cdot 3H_2O$	H_2	Rh	[79]
			3.5 nm	
$[C_4C_1Im][BF_4]$	$CoCl_2 \cdot 6H_2O$	$NaBH_4$	Co	[80]
		Ultrasound	30 ± 5 nm	
	$Cu[OCH(Me)CH_2NMe_2]_2$	Microwave heating, intramolecular red. or IL	Cu	[81]
			3.3 ± 0.9 m	
	$Cu(OAc)_2 \cdot H_2O$		Cu_2O nanocubes	
			43 ± 15 nm	
	Cu(I)-amidinate	Microwave heating, intramolecular red. or IL	Cu	[82]
	Zn(II)-amidinate		11 ± 6 nm	
	$[Cu\{MeC(N^iPr)_2\}]_2$		Zn	
	$[Zn\{MeC(NiPr)_2\}]$		3 ± 1 nm	
	$Ir_4(CO)_{12}$	Microwave heating,	Ir	[83]
			1.0 ± 0.4 m	
		electron beam	2.7 ± 0.7 nm	
$[C_4C_1Im][NTf_2]$	$(NH_4)_6Mo_7O_{24} \cdot 4H_2O$	$NaBH_4$	Mo	[84]
			10–50 nm	
			Bimetallic M-NPs	
$[C_4C_1Im][BF_4]$	$Fe_2(CO)_9$	Thermal decomposition	FeRu	[85]
	$Ru_3(CO)_{12}$		1.65 ± 0.3 nm	
	Cu(I)-amidinate	Microwave heating, intramolecular red. or IL	β-CuZn	[82]
	Zn(II)-amidinate		51 ± 29 nm	
	$[Cu\{MeC(N^iPr)_2\}]_2$		γ-Cu_3Zn	
	$[Zn\{MeC(NiPr)_2\}]$		48 ± 12 nm	
	$Ni(COD)_2$	H_2	NiGa	[86]
	$Ga(C_5Me_5)$		14 ± 5 nm	
	Triple-decker ruthenocene,	Microwave heating, intramolecular red. or IL	RuSn	[87]
	Anionic ruthenocene		4.3 ± 1.5 nm	
$[C_4C_1Im][NTf_2]$	$Co(acac)_3$	Thermal decomposition, intramolecular red. or IL	CoPt-nanorods	[88]
	$Pt(acac)_2$		8 nm	
	$[Ru(COD)(COT)]$	H_2	RuCu	[89]
	[CuMes]		1.9–2.8 nm	
$[C_4C_1Im][PF_6]$	$HAuCl_4$	$NaHB_4$	PdAu	[90]
	K_2PdCl_4	H_2	5.3 ± 3.0 nm	

Electrostatic and van der Waals interactions are present in nearly all colloidal and nanoparticular systems [97]. DLVO theory assumes flat surfaces of the particles and a homogeneous charge density, even upon approach of the particles. The concentration of the counter-ions, which cause the electric potential, is taken as constant. DLVO theory treats anions as ideal point charges. The influence of the solvent is considered only through its dielectric constant. DLVO theory is fundamental for colloids and predicts very well the stability of lyophobic colloids [98].

Ionic components as in surfactants or ionic liquids will generate an ionic double or Debye layer around the NPs (Fig. 3) resulting in electrostatic repulsion between equally surrounded NPs which will prevent the aggregation of the NPs in the dispersion. The effectiveness of such an electrostatic stabilization depends on parameters like pH, temperature, and concentration [92, 99]. Electrostatic repulsion is an important contribution for the stabilization of NPs using ionic compounds. The outer part of the ionic double layer may be formed by the bulky and less surface-coordinating alkyl ammonium, sulfonium, phosphonium, and imidazolium moieties which then add a steric stabilization (see below) [8].

For metal nanoparticles the anion of an original metal salt precursor has to be taken into account as electrostatic stabilizer. Small halide anions come closest to the "DLVO-type" point charge electrostatic stabilizers. DLVO theory predicts that the anion charges should be the primary source of stabilization for the unsaturated, electrophilic and possibly positively charged metal nanoparticles [100, 101]. The metal nanoparticles and their anion layer on the surface form then an overall negatively charged particle and are subject to Coulomb repulsion within the DLVO theory [47].

The stability of a colloid increases with the thickness of the Debye layer, which is the sum of the layers of counter-ions surrounding the particle. A thicker Debye layer stabilizes the particles by increasing the distance between them and reducing their van der Waals attraction. Also, the stability of colloids increases with the dielectric constant of the medium [102].

Limits of the DLVO theory are that it can only be applied to dilute systems ($<5 \times 10^{-2}$ mol/L) and cannot be applied to multiply charged ions or to sterically stabilized systems [103]. DLVO theory needs to be extended for effects such as hydrogen bonding, the hydrophobicity and steric interactions.

4.2 Steric Stabilization

Another important contribution in preventing aggregation of metal NPs is steric stabilization. Coordinating capping ligands like thiols, carboxylates, alcohols, long-alkyl-chain surfactants or polymers/oligomers act more or less through this type of stabilization [8].

When two nanoparticles enclosed by polymers or surrounded by long alkyl chains of ligands adsorbed on their surface approach each other, the polymer or alkyl chain layers will be compressed which results in a strong repulsion which is termed steric stabilization [104]. Steric repulsion derives from combination of entropic and osmotic contributions. The entropic part stems from a volume

restriction effect that decreases the number of possible configurations in the compressed region. The osmotic effect is due to an increase in concentration of the adsorbed polymers or ligand in the region between the two nanoparticles surfaces as they approach closer. Steric interactions in colloidal dispersions in molecular solvents have been extensively studied [104–108].

4.3 Combination of Both Electrostatic and Steric Stabilization

Compounds which stabilize both through electrostatic and steric effects are, for example, surfactants with long alkyl chains, such as cetyltrimethylammonium bromide (CTAB) or its gemini derivatives (cf. Fig. 2) [38–42], polymers containing ionic charges such as carboxyl-terminated poly(ethylene glycol) [93] or ionic liquids (see below). From theoretical and experimental studies, it became evident that the effectiveness of electrostatic stabilization increases with increasing particle size, whereas the effectiveness of steric stabilization increases with decreasing particle size [109]. The combination of electrostatic and steric stabilization is also referred to as *electrosteric* stabilization.

5 Stabilization of Metal Nanoparticles in Ionic Liquids

5.1 Electrostatic and Steric = Electrosteric Stabilization

ILs offer an interesting potential for stabilizing materials in the synthetic process. Their low interface energy is favorable for stabilizing small particles. ILs consist of cations and anions, which can act as electrostatic stabilizing agents. The IL ions or ion clusters are attracted to the nanoparticle surface by electrostatic forces [110]. The nature of the immediate ion layer around metal nanoparticles in ILs is still a matter of debate. DLVO theory predicts that the anion charges should be the primary source of stabilization for the unsaturated, electrophilic and probably positively charged metal nanoparticles [100, 101]. The metal nanoparticles and their anion layer on the surface would then form an overall negatively charged particle and are subject to Coulomb repulsion within the DLVO theory [47]. On the other hand, there are statements that the ionic liquid cations are attracted to the surface of a negatively charged nanoparticle to form a positive ion layer, and then counter-anions form a second layer on the nanoparticle surface by electrostatic attraction [111–113].

Palladium nanoparticles, which were grown onto multiwalled carbon nanotubes modified with imidazolium groups were claimed to be stabilized by the electrostatic interaction occurring between the imidazolium cations and the nanoparticle surface due to a coordination involving the imidazolium cation [114]. Upon exchange of the imidazolium counter-anion from Br^- and $[SbF_6]^-$ to $[NTf_2]^-$ no change in the material structure was noticed, i.e. no separation of the nanoparticles from the multiwalled carbon nanotubes [114]. Also, results from an X-ray photoelectron spectroscopy (XPS) investigation of functionalized imidazolium ILs with gold or platinum nanoparticles were seen to support this cationic coordination mode. Three

Fig. 4 Schematic proposed stabilization possibilities between metal nanoparticles and functionalized imidazolium cations [115]
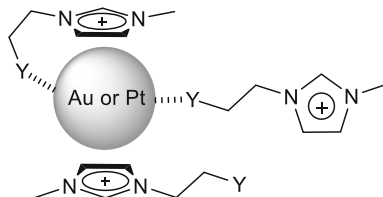
possible interactions, involving either the functional group and/or the imidazolium ring were proposed (Fig. 4) [115].

On the other hand, an XPS and an extended X-ray fine structure spectroscopy study (EXAFS) of iridium or platinum nanoparticles in the imidazolium ILs [C$_4$C$_1$Im][BF$_4$], [C$_4$C$_1$Im][PF$_6$] and [C$_4$C$_1$Im][OTf] showed interactions of the ionic liquid with the metal surface and the formation of an ionic liquid protective layer surrounding the metal particles [116, 117]. With small-angle X-ray scattering (SAXS) a variation in the protective layer length, from 2.8 to 4 nm, was evidenced depending on the type of anion. Moreover, the XPS analyses proved that the interaction between the metal surface and the IL occurs through F$^-$, when the anion is [BF$_4$]$^-$ of [PF$_6$]$^-$ or through O with the triflate, [CF$_3$SO$_3$]$^-$ anion [116, 117]. Consequently, one would assume that the ionic multilayer is composed of anions located immediately adjacent to the nanoparticle surface (Fig. 5) [166].

Density functional theory (DFT) binding energy (BE) calculations in a gas phase model favor interactions of Au$_n$ clusters ($n = 1, 2, 3, 6, 19, 20$) between IL anions, such as [BF$_4$]$^-$, instead of imidazolium cations. This suggests an Au⋯F interaction and anionic Au$_n$ stabilization in fluorous IL-anions [119]. Free imidazole bases (*e.g.* 1-methylimidazole) show similar binding energies. The Cl$^-$ anions have the highest binding energy and can therefore be expected to bind to the NP if present in the solution. At the same time no significant binding of the [C$_4$C$_1$Im]$^+$ or [HC$_1$Im]$^+$ imidazolium cations was found. These findings support the model of preferred interaction between anions and Au-NPs, but also confirm the importance to consider a possible presence of Cl$^-$ anions in the ionic liquid solution [74, 119].

The DFT study used the binding energy (BE) of different IL-ions, free bases and the Cl$^-$ anion to gold clusters of various sizes as a relative measure for the interaction strength. The BE is defined as the difference of the relaxed energies of the gas phase anions and the Au$_n$ clusters to the energy of their adduct (Eq. 1) [74, 119].

$$\text{BE} = E(\text{substrate, i.e., anion, free base or cation}) + E(\text{M}_n \text{with M} = \text{Au, Pd}) - E(\text{substrate adduct to M}_n).$$

(1)

Figure 6 shows the Au$_n$–IL anion binding configurations and the variation of the BE with cluster size n. Figure 7 illustrates other substrate–Au$_n$ binding configurations and the variation of the BE with cluster size n for [BF$_4$]$^-$ in comparison with other common substrate ligands. The BE of [C$_4$C$_1$Im]$^+$ is very weak and not included here [74, 119]. The BE of [C$_4$C$_1$Im]$^+$ is only 0.35 eV towards Au$_6$ or
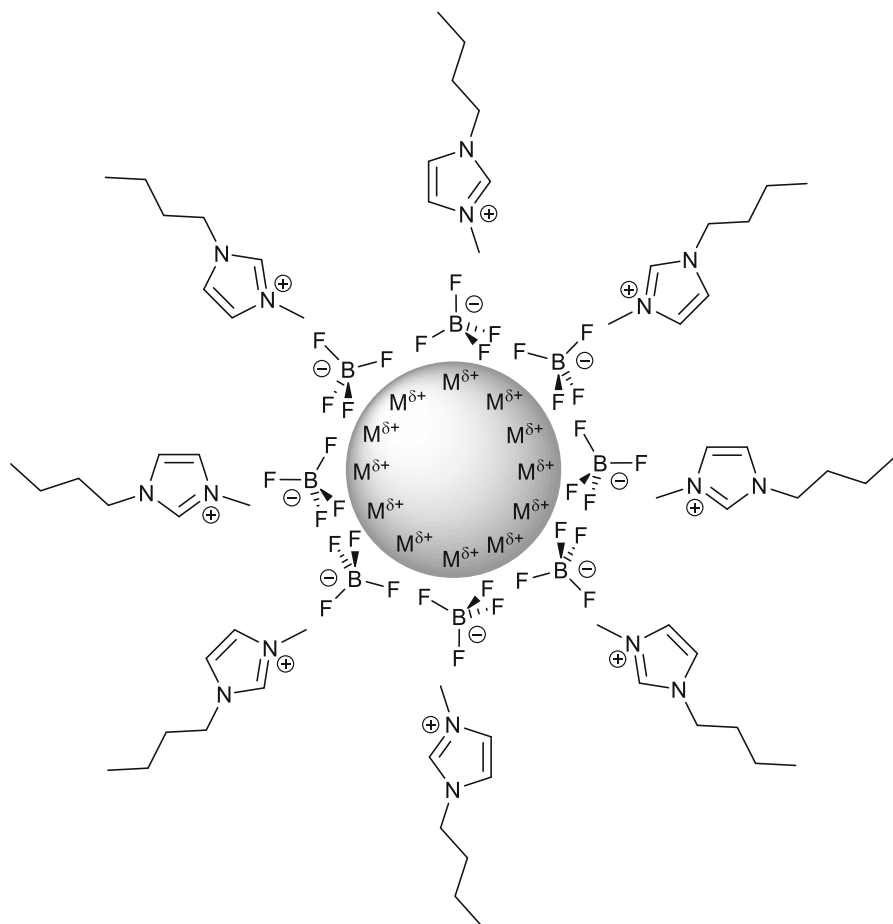
Fig. 5 Schematic depiction of proposed interactions between immediate IL anions, shown here for $[BF_4]^-$ anions and the metal nanoparticle surface with the IL-cations forming the second shell of the ionic double layer around a metal nanoparticle [118]

0.43 eV towards Au_{19} while the BE of $[BF_4]^-$ towards Au_6 and Au_{19} is 1.08 and 1.2 eV, respectively (1 eV = 23.06 kcal/mol). The BE comparison with chloride, citrate, PH_3 and H_2O illustrates the critical influence of the ionic charge and electron delocalization from the ligand to Au_n (Fig. 7). The softer the anion or ligand, that is, the more charge transfer or electron delocalization (according to Pearson's hard-soft concept and the nephelauxetic series) [120] to Au_n is possible, the better the stabilizing effect. H_2O as a hard and neutral ligand offers the least stabilization, hence, reduction of gold salts by $SnCl_2$ in water led immediately to the red purple solution (known as the Purple of Cassius). Remarkably, the relatively soft chloride anion shows the largest BE in agreement with the strong covalent binding of chloride ions to the Au(111) surface found in recent DFT simulations [121].
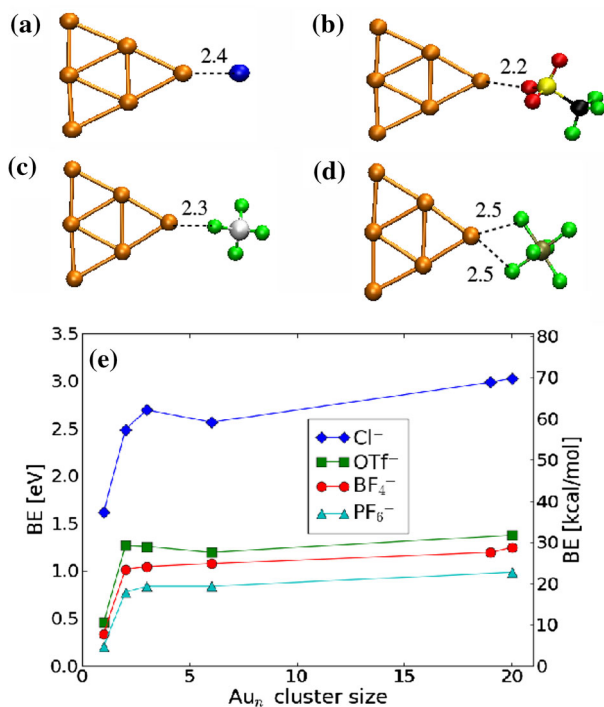
Fig. 6 Relaxed configurations of Au_6 bound to **a** Cl^-, **b** $[OTf]^-$, **c** $[BF_4]^-$ and **d** $[PF_6]^-$. The bond lengths are given in Å. **e** Binding energy. All the anions show a similar behavior in their BE: The BE to a single gold atom $n = 1$ is quite low and more than doubles for Au_2 ($n = 2$), therefrom is stays rather invariant with increasing the cluster size to $n = 20$, i.e., the BE is already saturated for Au_2. The chloride anion shows the largest BE of all anions and can be expected to bind to the clusters if it is present in the dispersion. Reprinted with permission from the author of Ref. [119]. Copyright Wiley–VCH 2009

A later combined DFT/vibrational spectroscopy approach found that palladium nanoparticles interact more strongly with the $[BF_4]^-$ anions than with the 1,3-dimethylimidazolium ($[C_1C_1Im]^+$) and 1-ethyl-3-methylimidazolium ($[C_2C_1Im]^+$) cations of the considered ILs. This suggested an important role of the anions in Pd-NP formation and stabilization in ILs. At the same time, the binding between isolated Pd atoms and the C atoms of the 1,3-dimethylimidazolium cation is stronger than Pd–$[BF_4]^-$ binding [122].

A similar DFT binding energy (BE) calculation with the 1-(2′-hydroxylethyl)-3-methylimidazolium cation $[HOC_2C_1Im]^+$ and a Pd_5 cluster pointed to the interaction of Pd_5 lying above the plane of the imidazolium ring and being in short contacts with C4 and C5 atoms of the imidazolium moiety and the oxygen atom of the hydroxyl group [123]. Yet, even with the added interaction of the functional hydroxyl group the binding energy is ca. 11 kcal/mol smaller than the BE of $[BF_4]^-$ anion to the Pd_5 cluster, suggesting a less important role of the cations with respect to stabilization of Pd-NPs relative to the role of the anions. This is in agreement with the above BE results, obtained earlier, for the Au_n clusters [119].
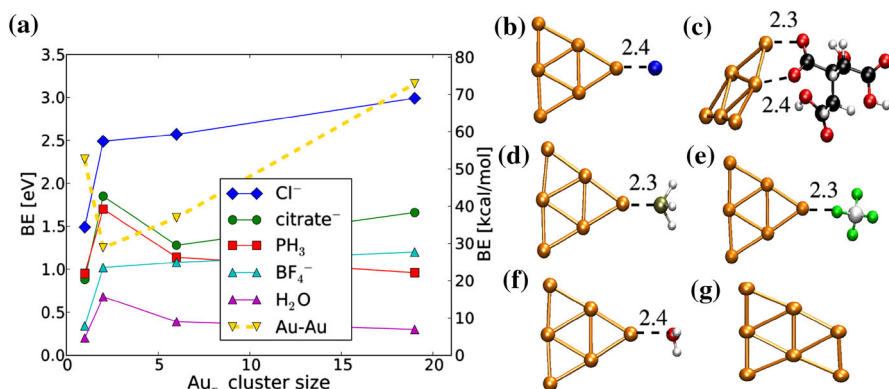
Fig. 7 **a** Binding energies (BE) and Au-atom addition energies depending on the cluster size. **b–f** Relaxed configurations of Au_6 bound to **b** Cl^-, **c** citrate$^-$ ($C_6H_7O_7^-$), **d** PH_3, **e** BF_4^- and (f) H_2O. **g** Relaxed configuration of Au_7. The bond lengths are in Å [74]. Reproduced from Ref. [74] with permission, copyright 2010 The Royal Society of Chemistry

The order of the calculated BEs was obtained for interaction energies between a Pd_5 cluster and the anions was $[CF_3CO_2]^-$ (~ 47 kcal/mol) > $[BF_4]^-$ (~ 41 kcal/mol) > $[OTf]^-$ (~ 34 kcal/mol) > $[PF_6]^-$ (~ 31 kcal/mol) $\cong [NTf_2]^-$ (~ 31 kcal/mol) [124].

For further examples of cation and anion effects on the formation of metal nanoparticles in ILs, see also the separate section on "cation and anion effects" below.

The IL-cations with alkyl chains can further contribute to the steric stabilization of nanoparticles. If the ionic liquid cation contains a long alkyl side chain, e.g., from imidazolium- or pyrazolium-based cations, the cations on or near the nanoparticle surface can provide steric forces by stretching out their bulky side-chains, thus hindering the nanoparticles from approaching each other (cf. Figure 5) [125]. ILs can also be designed with functional coordinating groups primarily in the alkyl chains of the cations, which thereby act as coordinating capping ligands (see Sect. 6 with Fig. 12 below) [126].

As noted above for stabilizing ionic components the cations and anions of ionic liquids, possibly as charged ion clusters, will surround the nanoparticle surface to build an electric double-layer, thus providing an electrostatic force to keep the nanoparticles apart from each other [65]. The role of electrostatics in stabilizing the nanoparticles in ionic liquids has been well recognized [115, 127–133].

The interaction energies of ILs with different cations and anions to Ru-NPs were compared by titration calorimetry and by molecular simulation. Structural information from the molecular simulation suggests that the charged parts of both the IL cation and the anion are in contact with the surface of the nanoparticle, with only small charge separation at the interface. The results of this study suggest an IL-dependent balance between electrostatic, van der Waals, and H-bond forces for the stabilization of metal nanoparticles [128].

For nanoparticles in ionic liquids, steric stabilization can emerge from bulky groups in the IL cation (or anion) and/or from the addition of macromolecules, both of which hinder nanoparticles from contacting each other and from aggregation [125]. When only small amounts of polymer are added to the nanoparticle–ionic liquid dispersion, the nanoparticle surfaces are partially covered by polymers and polymer coils extend from one particle surface to another particle. Thereby, the polymers chains can function as bridges between nanoparticles. As an excess of polymer is added, the polymers can fully cover the nanoparticle surface to form an adsorbed polymer layer [134]. Then steric repulsion and stabilization arises from the adsorbed polymer layers of neighboring nanoparticles as noted above. Block copolymers have been utilized to stabilize nanoparticle dispersion [105]. PEO–PPO–PEO block copolymer Pluronic P123 ($EO_{20}PO_{70}EO_{20}$) formed a lamellar lyotropic liquid crystal structure in pyrrolidinium nitrate ([Pyrr][NO_3]) ionic liquid at the 58–82 wt% polymer concentration range. Gold nanoparticles were prepared by reducing $HAuCl_4$ in this lyotropic liquid crystal [135].

Various and also yet unknown factors influence the stability of nanoparticles in ionic liquids and lead to nanoparticle size [136–139] and/or morphology [140–145] changes during synthesis. Smaller diameter and narrower distributions of synthesized nickel metal and zinc oxide nanoparticles were prepared in ionic liquids with longer side chains [137, 141]. Larger size or varied morphologies of synthesized nanoparticles can be caused by conglomeration of unstable primary nanoparticles, which may result from smaller ionic liquid anions exhibiting stronger cation–anion Coulomb attraction [145], or less coordinating anions of ionic liquids [116, 144] or higher temperature decreasing the viscosity of the ionic liquid and increasing the diffusive velocities of the nanoparticles [146, 147]. An improved understanding of the stability of nanoparticle dispersions in ionic liquids is still needed to assist efforts directed toward the synthesis of nanoparticles with controlled size and morphology in ionic liquids [125].

5.2 Hydrogen Bonding Interactions

Imidazolium cations through their imidazolium-C–H groups can form hydrogen bonds to the fluorine or oxygen atoms of the IL anions [148–150] that induce structural directionality (IL effect). This is different from tetraalkylammonium ILs that, by contrast, display charge-ordered structures. The ILs act as stabilizing media, but importantly also display self-organization on the nanomolecular scale. The imidazolium ILs form extended hydrogen-bond networks at the liquid state and therefore are by definition ''supramolecular'' fluids. This structural organization of ILs can be used as ''entropic drivers'' (the so-called ''IL effect'') for the spontaneous, well-defined and extended ordering of nanoscale structures. The properties of especially the imidazolium-based ILs are based on their formation of aggregates rather than on their isolated cations and anions [151, 152]. The structures of 1,3-dialkylimidazolium salts form an extended network of cations and anions connected together by hydrogen bonds in the condensed phase, which is maintained to a great extent in the gas phase [152].

Thus, hydrogen bond interactions are present in imidazolium-based ionic liquid nanoparticle dispersions in addition to electrostatic, van der Waals and steric interactions [153, 154]. Metal nanoparticles can possess hydroxido and/or oxido ligands on their surface, which can also hydrogen bond with ionic liquids [155]. Such metal-surface bound oxygen species can be derived from crystal water of the metal salt precursor (cf. Table 1), from difficult to remove residual water in the IL or from gaseous dioxygen (as impurity even when working under inert gas). The IL-cation–anion hydrogen bond and NP–IL hydrogen bond compete with each other and contribute to nanoparticle stabilization in ionic liquids, as shown in Fig. 8 [156, 157].

The interaction energies of ILs with an additional alkyl group in the C-2 position of the imidazolium cation ($[C_4C_1C_1Im][NTf_2]$ with 1-butyl-2,3-dimethylimidazolium) and a N-butyl-N-methylpyrrolidinium cation ($[C_4C_1Pyrr][NTf_2]$) to Ru-NPs were compared to other $[C_nC_1Im]^+$-ILs by titration calorimetry and by molecular simulation. Ionic liquids with cations which are less likely to form hydrogen bonds such as $[C_4C_1C_1Im]^+$ or $[C_4C_1Pyrr]^+$ also interact less favorably with Ru-NPs [113].

Qualitative direct comparison (for the same IL-anion) of an IL with the $[C_4C_1Im]^+$-cation which has hydrogen-bonding possibility and a cation with no significant H-bond formation reveals the former to be better stabilizers for Au- or Cu-NPs whereas in the latter ILs fast particle growth and agglomeration was observed [156]. The stable time of the colloidal dispersion in $[C_4C_1Im][N(CN)_2]$ and trihexyltetradecylphosphonium dicyanamide $[P_{66614}][N(CN)_2]$ was 3 days versus 1 day. In $[C_4C_1Im][BF_4]$ or $[C_4C_1Im][NTf_2]$ Au-NPs were stable for 1 week while in N-butyl-N-methyl-pyrrolidinium, $[C_4C_1Pyr][NTf_2]$ or in N-butyl-pyridinium$[C_4Py][NTf_2]$ fast precipitation occurred due to fast particle growth and agglomeration [156].
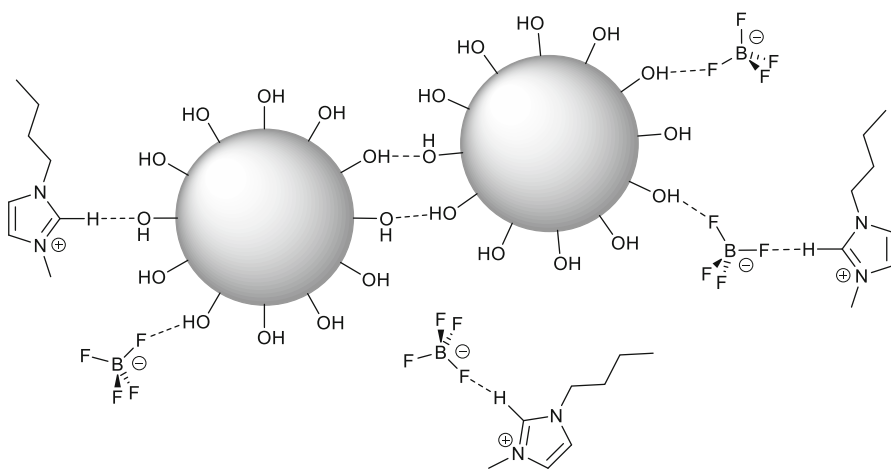
Fig. 8 Hydrogen bonds formed between the surface hydroxyl-groups of metal nanoparticles and ions of ionic liquids and between cations and anions of ionic liquids

5.3 Influence of Polar and Non-Polar Domains in ILs

The segregation of hydrophilic or hydrophobic regions, polar and non-polar domains in imidazolium-based ILs is an important physicochemical property which effects their solvation and interaction with dissolved species (Fig. 9) [158–160]. Expectedly polar substrates, like metal salts are preferentially dissolved in polar domains and non-polar compounds like organometallic precursors in non-polar IL regions [159, 161]. Consequently, the nature of the metal precursor—ionic or neutral for instance—is also a key determinant of the size and shape of the prepared metal NPs as the polarity and the volume of these IL nanoregions may modulate this. The nanoparticle growth process is probably controlled by the local concentration of the precursor and possibly limited to the size and shape of the IL polar or non-polar domains (Fig. 9) [65].

5.4 Cation and Anion Effects

Nanoparticle preparation in ILs is often accompanied by heating to over 100 °C or even 200 °C. Changing the anions or the cations can have a strong influence on the thermal behavior, density, viscosity (see below), or conductivity [160]. For example, the simple sum of the cationic and anionic self-diffusion coefficients ($D_{cation} + D_{anion}$) for selected room temperature ILs follows the (anion) order $[C_4C_1Im][NTf_2] > [C_4C_1Im][CF_3CO_2] > [C_4C_1Im][OTf] > [C_4C_1Im][BF_4] > [C_4C_1Im][(F_5C_2SO_2)_2N] > [C_4C_1Im][PF_6]$ at 30 °C. This order of the diffusion coefficients is as expected the reverse of the order of the viscosity (see below). The degree of ionic association can be estimated from the ratio of the molar conductivity obtained from the impedance measurement (Λ_{imp}) and the molar conductivity calculated from the ionic diffusivity (Λ_{NMR}). For the anions at the given $[C_4C_1Im]^+$ cation the degree of association increases according to $[PF_6]^- < [BF_4]^- < [(F_5C_2SO_2)_2N]^- < [NTf_2]^- < [OTf]^- < [CF_3CO_2]^-$. In the order from $[PF_6]^-$ to $[NTf_2]^-$ electronegative fluorine atom and electron-withdrawing perfluorosulfonyl groups contribute to the distribution of the anionic
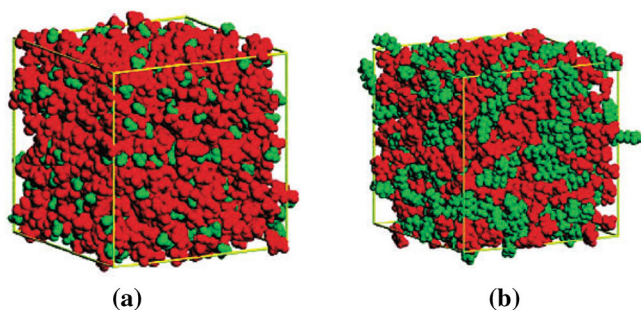

Fig. 9 Simulation study of two imidazolium-based hexafluorophosphate ILs (each *box* contains 700 ions) showing polar (*red*) and non-polar (*green*) domains for **a** 1-ethyl-3-methylimidazolium, $[C_2C_1Im]^+$ and **b** 1-methyl-3-*n*-octylimidazolium $[C_8C_1Im]^+$. Reprinted with permission from Ref. [162]. Copyright 2006 American Chemical Society

charge. Also, the surface coverage of the anion backbone by fluorine atoms may be a significant factor for only weak interactions with the $[C_4C_1Im]^+$ cation. Whereas, the relatively higher anionic charge localization in $[OTf]^-$ (=$[CF_3SO_3]^-$ and $[CF_3CO_2]^-$) leads to their stronger interaction with the $[C_4C_1Im]^+$ cation [160]. The interaction energies of ILs with $[C_4C_1Im]^+$ and the anions $[NTf_2]^-$ or $[PF_6]^-$ were compared by titration calorimetry and by molecular simulation to Ru-NPs. No significant differentiating effect of the two anions was observed. Structural information from the molecular simulation suggests that the charged parts of both the IL cation and the anion are in contact with the surface of the nanoparticle, with only small charge separation at the interface [128]. The relative order of anion stabilities for ILs with the $[C_1C_4Im]^+$ cation was observed as $[NTf_2]^-$ > $[PF_6]^-$ > $[BF_4]^-$ ≫ Cl^- [163].

The size of M-NPs was found to increase with the molecular volume of the anion of the IL. Metal nanoparticles synthesized in $[C_4C_1Im]^+$ ILs increased in size with the size of the IL-anion from small $[BF_4]^-$ over $[OTf]^-$ to the large $[NTf_2]^-$ anion [20, 164, 165]. The IL-anion molecular volume was taken as the size of the IL-anion. The effect was shown for Rh- [164], Ag- [20] and W-NPs [165]. Figure 10 depicts the correlation between the nanoparticle size of W- and Rh-NPs and the molecular volume of the anion.

The influence of the anion to metal nanoparticles was also observed by several other research groups [116, 167–170]. 1-*n*-Butyl-methyl-imidazolium salts $[C_4C_1Im]^+$ with weakly coordinating perfluorinated counter anions ($[BF_4]^-$, $[PF_6]^-$ or $[NTf_2]^-$) were qualitatively found to be better stabilizers compared to ILs with anions of higher coordination strength (dicyanamide, $[N(CN)_2]^-$). In the former ILs Au- or Cu-NPs were stable colloidal dispersions, that is, without precipitation or aggregation for 1 week to several weeks. In $[C_4C_1Im][N(CN)_2]$ Au-NPs were stable for only 3 days due to fast particle growth and agglomeration [156].

The IL-anion had an effect on the dissolution and reaction rate when fabricating copper nanoparticles from Cu flakes (of 1–5 μm) in ILs [171]. When $[C_4C_1Im][BF_4]$, $[C_4C_1Im][PF_6]$ and $[C_2C_1Im][BF_4]$ were used, it took a relatively long
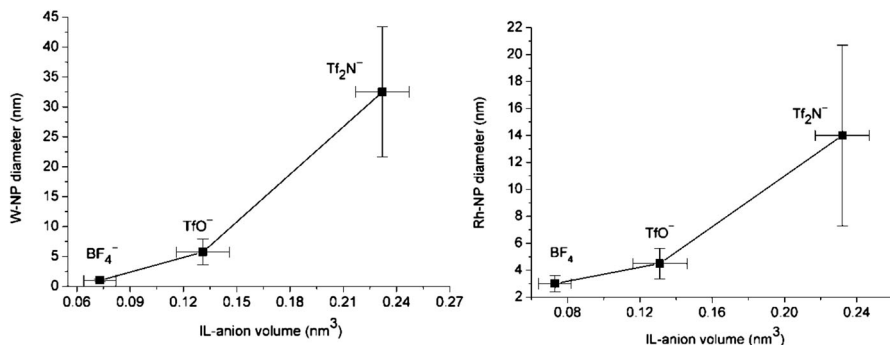
Fig. 10 Correlation between nanoparticle size of W- and Rh-NPs from TEM measurements and the IL anion molecular volume with standard deviation (1σ) as *error bars* [164, 165]. Left part is reproduced from Ref. [165] with permission, copyright 2008 The Royal Society of Chemistry; right part is adapted from Ref. [164] with permission, copyright 2009 Elsevier B.V.

time, of 24 h to obtain the copper nanoparticles while in [C$_4$C$_1$Im][NO$_3$] dissociation of Cu flakes to Cu nanoparticles took place in about 5 min. It was suggested that the favorable interaction between free nitrate anion of [C$_4$C$_1$-Im][NO$_3$] and the Cu metal surface caused the flakes to dissociate in the ionic liquid, forming as much smaller nanoparticles than in the other ILs. From TEM the average diameter of the obtained Cu-NPs in [C$_4$C$_1$Im][NO$_3$] was 10 nm [171] while the size range in [C$_4$C$_1$Im][BF$_4$] was 50–100 nm [172] or 20–200 nm [124] and in [C$_4$C$_1$Im][PF$_6$] and [C$_2$C$_1$Im][BF$_4$] it was 80–100 nm [172]. Overall, these results suggested that the pristine micro-sized copper flakes were already clusters of primary nanoparticles, which were dis-agglomerated to nanoparticles by introduction in ILs to a different extent.

Decomposition of Pd(OAc)$_2$ in a series of hydroxyl-functionalized ionic liquids (ILs) with the 1-(2′-hydroxylethyl)-3-methylimidazolium cation [HOC$_2$C$_1$Im]$^+$ and the anions [BF$_4$]$^-$, [PF$_6$]$^-$, [OTf]$^-$ [CF$_3$CO$_2$]$^-$ ([ATf]$^-$) or [NTf$_2$]$^-$ gave Pd-NPs with slightly different medium diameters from 2.3 ± 0.4 nm in [HOC$_2$C$_1$Im][ATf] or 2.4 ± 0.5 nm in [HOC$_2$C$_1$Im][OTf] to 4.0 ± 0.6 nm in [HOC$_2$C$_1$Im][BF$_4$] [124]. Noteworthy from comparison with the non-functionalized IL, [C$_4$C$_1$Im][NTf$_2$] (medium diameter 6.2 ± 1.1 nm) significantly smaller nanoparticles were obtained. More importantly, the ease of formation of the Pd-NPs in the [HOC$_2$C$_1$Im]$^+$-based ILs followed the order [NTf$_2$]$^-$, [PF$_6$]$^-$ > [BF$_4$]$^-$ > [OTf]$^-$ > [ATf]$^-$ based on the residual unreacted amount of Pd(OAc)$_2$ in the dispersion. This order does not relate to the stability towards aggregation. For this, it could only be noted that in [HOC$_2$C$_1$Im][PF$_6$] a series of larger Pd-NPs over 8 nm (compared to the average 3.1 ± 0.7 nm) were also present and the Pd-NPs were least stable in this [PF$_6$]$^-$ IL. From the ratio of metallic Pd to PdO observed in the XPS the relative resistance of the Pd-NPs towards oxidation may be determined. The ability of the [HOC$_2$C$_1$Im]$^+$-ILs to prevent the Pd NPs from undergoing oxidation follows the trend [NTf$_2$]$^-$ > [-PF$_6$]$^-$ > [ATf]$^-$ > [OTf]$^-$ > [BF$_4$]$^-$. For example, only 12.6% of PdO was present in the NPs isolated with the [NTf$_2$]$^-$-anion whereas nearly half the Pd amount was oxidized to PdO in the case of the [BF$_4$]$^-$-anion. Studies for [PF$_6$]$^-$ and [NTf$_2$]$^-$ showed that these are the least nucleophilic anions [173] and also the most hydrophobic ones in the series while [BF$_4$]$^-$ is the least hydrophobic/most hydrophilic one of the anions used in this comparison. Therefore, the oxidation-protecting effect may be accounted for by the fact that water and oxygen are repelled most by the [PF$_6$]$^-$ and [NTf$_2$]$^-$ anions [124].

Strong anion effects were seen on gold nanoparticle formation in ionic liquids of [C$_2$C$_1$Im]$^+$ with ethyl sulfate ([EtSO$_4$]$^-$), [OTf]$^-$ and methanesulfonate ([CH$_3$SO$_3$]$^-$) anions [78]. Face-centered cubic gold nanoparticles were grown by reduction of HAuCl$_4$·3H$_2$O with glycerol at temperatures between 120 and 180 °C. The [CH$_3$SO$_3$]$^-$ anion yielded nanoparticles with diameters between 5 and 7 nm, which increasingly aggregate at higher reaction temperatures but the primary particle size is not affected. Thus, the [CH$_3$SO$_3$]$^-$ anion or more accurate the anion-cation ([C$_2$C$_1$Im]$^+$) combination under the given reaction conditions is able to efficiently trap very small gold nanoparticles. High temperatures like 180 °C do not lead to a further growth of the particles, but rather to a controlled aggregation. From [OTf]$^-$ also small 5–7 nm particles formed, but only at low temperatures whereas

above ca. 160 °C, large, ill-defined and aggregated particles were obtained. Apparently the [OTf]$^-$ anion is only partially able to stabilize small gold particles and above a certain reaction temperature the stabilization exerted by the IL is broken and led to larger aggregates. With the [EtSO$_4$]$^-$ anion polydisperse samples formed at all temperatures except 160 °C. In the temperature window around 160 °C individual, controlled ca. 15–20 nm particles were grown from [C$_2$C$_1$-Im][EtSO$_4$] [78].

It is evident from many reports on cation and anion effects of ILs that the interaction between an IL and a (growing) nanocrystal is far from understood but that a detailed understanding of the IL–nanoparticle interaction, of the thermodynamics and kinetics, and of the initial nucleation process would be needed for a more rational design of nanomaterials in ILs [78].

5.5 Alkyl Chain Effects

The interaction energies of ILs with different alkyl chain lengths ([C$_n$C$_1$Im][NTf$_2$] (n = 2, 4, 6, 8, 10)), an additional alkyl group in the C-2 position of the imidazolium cation ([C$_4$C$_1$C$_1$Im][NTf$_2$] with 1-butyl-2,3-dimethylimidazolium) and a N-butyl-N-methylpyrrolidinium cation ([C$_4$C$_1$Pyrro][NTf$_2$]) to Ru-NPs were compared by titration calorimetry and by molecular simulation. The interaction energy of [C$_n$C$_1$Im][NTf$_2$] (n = 6, 8, 10) with Ru-NPs is larger than that of [C$_4$C$_1$Im][NTf$_2$] indicating that longer alkyl side chains enhance the interactions with Ru-NPs. Here [C$_2$C$_1$Im][NTf$_2$] also has stronger interactions with the nanoparticles, but this deviation was explained by the cation not having a significant nonpolar moiety. Structural information from the molecular simulation suggests that the alkyl chains tend to point away from the surface but are still within interaction range [128].

Trends for the influence of the alkyl chain length were invoked by many other research groups [174–177] such that the alkyl chain length has an influence of the particle size of M-NPs [21, 174]. In the well-designed series of mono- and di-cationic imidazolium ILs with different alkyl chain length and [NTf$_2$]$^-$ as anion (Fig. 11) Ni-NPs were synthesized by spontaneous decomposition of [bis(1,5-cyclooctadiene)nickel(0)], Ni(COD)$_2$. Well dispersed Ni-NPs with a small mean size and narrow size distribution could be obtained. The Ni-NP size increased with increasing chain lengths from 2.4 ± 0.8 nm in [C$_{12}$C$_1$Im][NTf$_2$] over 2.9 ± 0.4 nm in [C$_{18}$C$_1$Im][NTf$_2$], 4.0 ± 0.5 nm in [C$_{12}$C$_{12}$Im][NTf$_2$] about equal to 4.4 ± 0.7 nm in [C$_{12}$C$_1$C$_{12}$Im][NTf$_2$], 5.4 ± 1.6 nm in [C$_{12}$Im-µ-C$_6$-ImC$_{12}$][NTf$_2$], (200 nanoparticle were measured in the first four cases, 50 NPs in the last case). When an ethereal oxygen donor atom was introduced in the functional IL [C$_{12}$Im-µ-C$_2$OC$_2$-ImC$_{12}$][NTf$_2$] the particle size decreased to 3.4 ± 0.2 nm (based on 200 NPs). In addition, formation of regularly interspaced NP arrays was also observed in such long chain ILs [174].

For Au-NPs in imidazolium-based ILs the particles diameter increases from 0.75 to 3.5 nm diameter for [C$_2$C$_1$Im]$^+$, [C$_4$C$_1$Im]$^+$ and [C$_8$C$_1$Im]$^+$ cations and [BF$_4$]$^-$ as counter ion [178, 179]. Further, decomposition of Ni(COD)$_2$ in [C$_n$C$_1$Im][NTf$_2$] ILs gave Ni-NPs with an average diameter from 2.4 to 5.4 nm [174] or 4.9 to
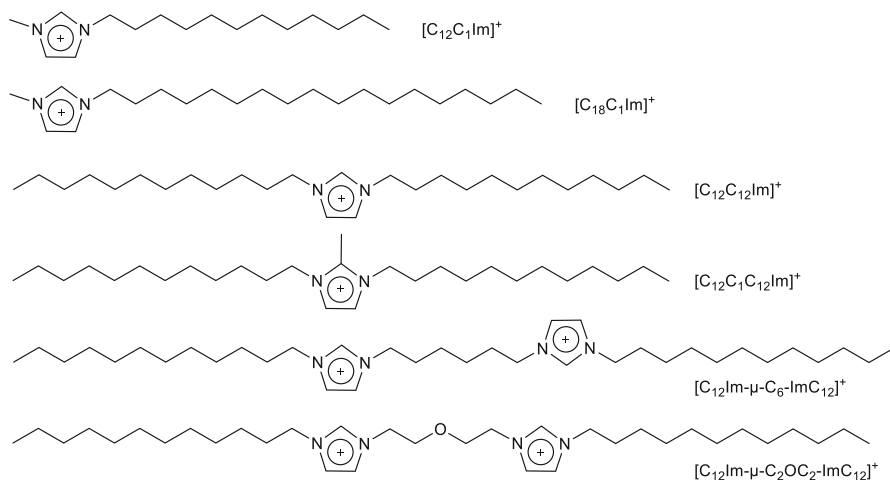
Fig. 11 Series of ionic liquid cations with increasing chain length and $[NTf_2]^-$ as the common anion used in the comparative synthesis of Ni-NPs from $Ni(COD)_2$ to elucidate the chain-length effect on the metal nanoparticle size [174]

5.9 nm [180] with conflicting trends such that the particle diameter increased or decreased with the cation size.

When interpreting such trends with seemingly small differences in nanoparticle size, the standard deviation σ of the size distribution must be considered, however. The, at first sight, slightly larger nanoparticle size may still well be within 1σ or certainly within 3σ of the average diameter of another size.

In another study, nickel nanoparticles were obtained by decomposition of $Ni(COD)_2$, again with different nanoparticle diameter, depending on the chain length of the imidazolium cation with $[NTf_2]^-$ as anion. The results were 5.9 ± 1.4 nm for $[C_4C_1Im]^+$, 5.6 ± 1.3 nm for $[C_8C_1Im]^+$, 4.9 ± 0.9 nm for $[C_{10}C_1Im]^+$, 5.1 ± 0.9 nm for $[C_{14}C_1Im]^+$ and 5.5 ± 1.1 nm for $[C_{16}C_1Im]^+$. While it may appear that an increase of the alkyl chain (from *n*-butyl to *n*-hexadecyl) induces the formation of nanoparticles with a smaller diameter and size-distribution, all distributions are strongly overlapped within their 1σ regions already. The differences in diameter and size distribution are relatively small and could be a TEM artefact (sample preparation and/or particle counting, for instance) as the authors admit themselves [180].

Table 2 illustrates that a change in imidazolium cation or rather in 1-*n*-alkyl chain length does not give a clear trend in the size of the Ni-NPs synthesized by nickel(II)-bis(amidinate) or $Ni(COD)_2$ precursor decomposition through microwave assisted heating. The size distributions overlap considerably already within the 1σ standard deviation. Only in the case of the $Ni(COD)_2$ precursor there is an indication of Ni-NP size increase from n-butyl over *n*-octyl to *n*-dodecyl which is reverse from the aforementioned trend [181].

In terms of stabilization, short alkyl-chain-methyl-imidazolium salts $[C_4C_1Im]^+$ with weakly coordinating perfluorinated counter anions ($[BF_4]^-$, $[PF_6]^-$ or $[NTf_2]^-$)

Table 2 Ni-NP diameter and distribution from different precursors and in different ILs	Ni-precursor[a], IL	TEM Ø (1σ) [nm][bc]
	[Ni(AMD)$_2$]	
	[C$_4$C$_1$Im][BF$_4$]	5 (±2)
	[C$_{12}$C$_1$MIm][BF$_4$]	7 (±2)
	[C$_4$C$_1$Im][PF$_6$]	7 (±4)
	[C$_8$C$_1$Im][PF$_6$]	7 (±1)
	[C$_{12}$C$_1$Im][PF$_6$]	9 (±3)
	[C$_4$C$_1$Im][NTf$_2$]	10 (±2)
	[C$_8$C$_1$Im][NTf$_2$]	10 (±3)
	[C$_{12}$C$_1$Im][NTf$_2$]	10 (±4)
	Ni(COD)$_2$	
	[C$_4$C$_1$Im][PF$_6$]	8 (±3)
	[C$_8$C$_1$Im][PF$_6$]	10 (±2)
	[C$_{12}$C$_1$Im][PF$_6$]	15 (±2)

[a] 1.0 wt. % Ni-NP/IL dispersions obtained by microwave-assisted heating with 100 W for 10 min at 220 °C

[b] The size distribution was calculated from a manual diameter determination over a minimum of 50 isolated particles

[c] Average diameter and standard deviation

were qualitatively found to be better stabilizers compared to ILs with cations bearing long alkyl chains (trihexyltetradecylphosphonium [P$_{66614}$]$^+$, 1-octyl-3-methylimidazolium [C$_8$C$_1$Im]$^+$) and anions of higher coordination strength (dicyanamide, [N(CN)$_2$]$^-$) (see above). In [C$_4$C$_1$Im]$^+$ with [BF$_4$]$^-$, [PF$_6$]$^-$ or [NTf$_2$]$^-$ anions Au- or Cu-NPs were stable colloidal dispersions, that is, without precipitation or aggregation for 1 week to several weeks. In [C$_4$C$_1$Im][N(CN)$_2$] Au-NPs were stable for 3 days. In comparison in [C$_8$C$_1$Im][PF$_6$] or in [P$_{66614}$][N(CN)$_2$] fast precipitation or stability for only 1 day, respectively, was observed due to fast particle growth and agglomeration [156].

5.6 Viscosity

Viscosity of the reaction medium can be expected to have a crucial influence on the growth and agglomeration of nanoparticles. Unfortunately, differences in viscosity cannot be treated separately from concomitant changes in alkyl chain length or anion. Thus, viscosity dependence for nanoparticle size and size distribution appears to be seldom addressed [64].

For example, for [C$_4$C$_1$Im]$^+$-ILs the viscosity at 30 °C follows the anion order [PF$_6$]$^-$ > [(F$_5$C$_2$SO$_2$)$_2$N]$^-$ > [BF$_4$]$^-$ > [OTf]$^-$ > [CF$_3$CO$_2$]$^-$ > [NTf$_2$]$^-$, which is as expected opposite to the order of the diffusion coefficients (see above).

For the [C$_n$C$_1$Im][BF$_4$] ($n = 2$, 4, 6) [182], [C$_n$C$_1$Im][PF$_6$] ($n = 4$–9) and [C$_n$C$_1$Im][NTf$_2$] ($n = 2$–10) series the viscosity increases with increasing the number n of carbon atoms in the linear alkyl chain in the imidazolium cation. However, the trends are quite different. An almost linear dependence of the viscosity as a function of the alkyl chain length group is observed for the [NTf$_2$]$^-$ ILs while the dependence for the [PF$_6$]$^-$ ILs is more like an exponential increase with a local maximum at $n = 7$. Also, the [C$_n$C$_1$Im][PF$_6$] ionic liquids are much more viscous than their [NTf$_2$]$^-$ analogs [183].

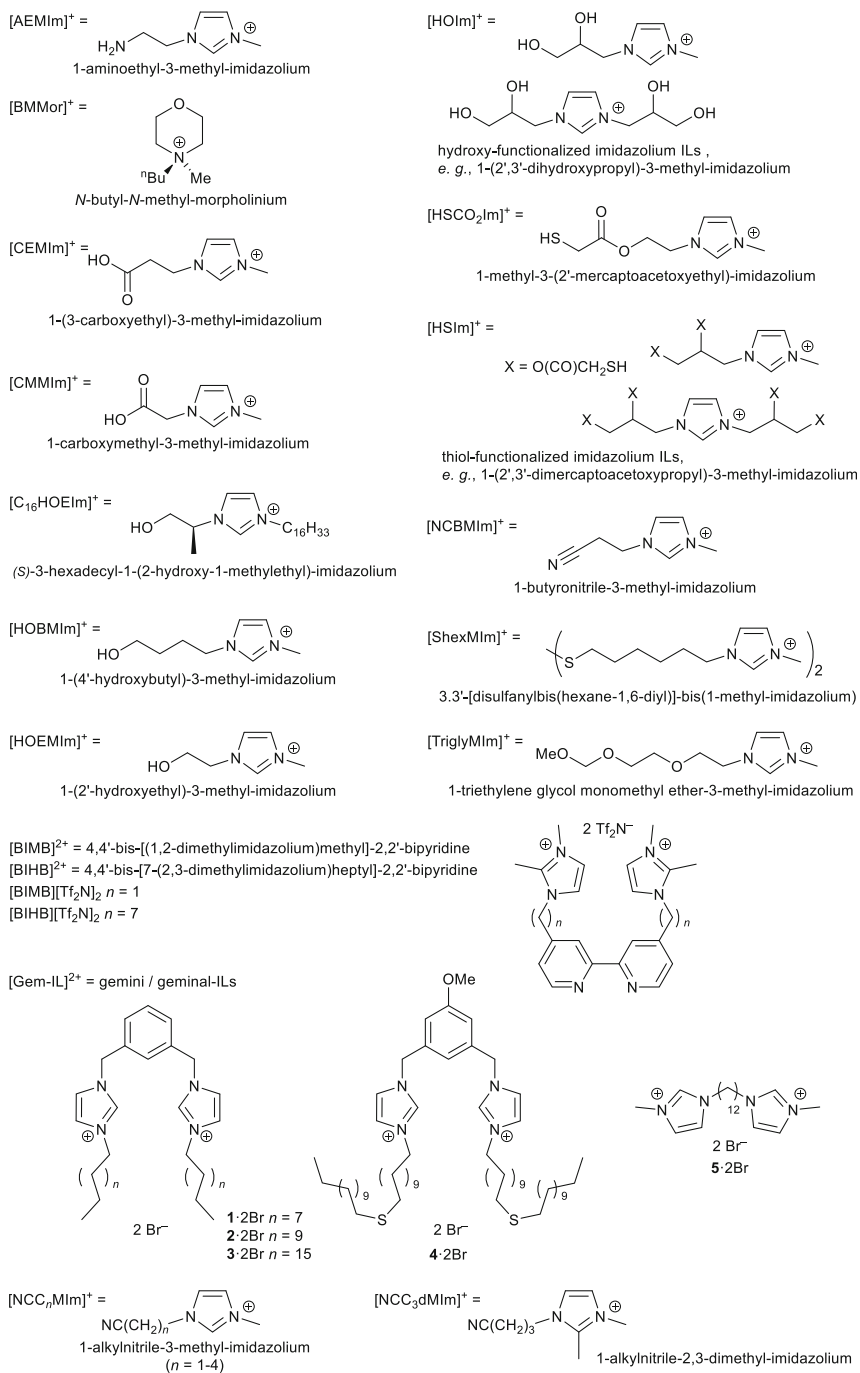# 6 Influence of Functional ILs to Metal Nanoparticles

Functionalized imidazolium ILs can be used to modify the surface of metal NPs [184, 185], in particular to provide stable dispersion of NPs in water [113, 186], which is important to many applications [187]. Thiol- [184, 188, 189], ether- [113], carboxylic acid- [115], amino- [190] and hydroxyl-functionalized imidazolium ILs are available (Fig. 12), for example, to prepare aqueous dispersions of noble metal NPs.

From comparison of the decomposition of $Pd(OAc)_2$ in a series of hydroxyl-functionalized ionic liquids (ILs) with the 1-(2′-hydroxylethyl)-3-methylimidazolium cation $[HOC_2C_1Im$ or HOEMIm$]^+$ and the anions $[BF_4]^-$, $[PF_6]^-$, $[OTf]^-$, $[CF_3CO_2]^-$ or $[NTf_2]^-$ and the non-functionalized IL, $[C_4C_1Im][NTf_2]$ it appeared that the hydroxyl group accelerated the formation of the NPs, and also helped to protect the NPs from oxidation once formed. Significantly smaller Pd-NPs were obtained in the [HOEMIm or $HOC_2C_1Im]^+$-ILs with average diameters from 2.3 ± 0.4 nm in the $[CF_3CO_2]^-$ salt to 4.0 ± 0.6 nm in the $[BF_4]^-$ analog while in non-functionalized $[C_4C_1Im][NTf_2]$ the average diameter was 6.2 ± 1.1 nm [124].

An X-ray photoelectron spectroscopic study of purified aminoethyl-methylimidazolium bromide, $[H_2NC_2C_1Im$ or AEMIm]Br-stabilized Au-NPs suggested that both the imidazolium ring and the functional amino group were involved in the interaction with the NP surface (cf. Figure 4) [115]. A shift in binding energies in the peaks of the carbon and nitrogen atoms in the imidazolium ring and amino N atom and a change in the width of the N1 s peak were observed. The XPS results were interpreted as either an electrostatic interaction between the imidazolium cation and the negatively charged metal surface, an interaction between the amino group and surface metal atom or the simultaneous coordination of the imidazolium cation and the functional group with the metal NPs. The electrostatic imidazolium-metal interaction would change the positive charge density of the imidazole ring. Amino group coordination to the metal NPs surface would induce a shift in N atom binding energies in the peak of the amino group and a change in the width of the N1 s peak [115].

Comparison between the closely related di-cationic ILs $[C_{12}Im-\mu-C_6-ImC_{12}][NTf_2]$, and $[C_{12}Im-\mu-C_2OC_2-ImC_{12}][NTf_2]$ (cf. Figure 11) revealed a significant decrease in Ni-NP size (obtained from spontaneous decomposition of $Ni(COD)_2$) from 5.4 ± 1.6 nm to 3.4 ± 0.2 nm when an ethereal oxygen donor atom was introduced. This indicates a better templating and stabilization effect due to coordination of the negatively polarized O-atom on the metal surface [174].

The synthesis of Co-NPs and Mn-NPs by microwave-heating induced decomposition of the metal carbonyls $Co_2(CO)_8$ and $Mn_2(CO)_{10}$, respectively, yields smaller and better separated particles in the functionalized IL 1-(3-carboxyethyl)-3-methyl-imidazolium tetrafluoroborate [CEMIm or $HO_2CC_2C_1Im][BF_4]$ (1.6 ± 0.3 and 4.3 ± 1.0 nm, respectively) than in the non-functionalized IL $[C_4C_1Im][BF_4]$. The particles are stable in the absence of capping ligands (surfactants) for more than 6 months although some variation in particle size could be observed by TEM (Fig. 13) [191].

[AEMIm]⁺ =

1-aminoethyl-3-methyl-imidazolium

[BMMor]⁺ =

ⁿBu   Me

N-butyl-N-methyl-morpholinium

[CEMIm]⁺ =

1-(3-carboxyethyl)-3-methyl-imidazolium

[CMMIm]⁺ =

1-carboxymethyl-3-methyl-imidazolium

[C₁₆HOEIm]⁺ =

HO   C₁₆H₃₃

(S)-3-hexadecyl-1-(2-hydroxy-1-methylethyl)-imidazolium

[HOBMIm]⁺ =

1-(4'-hydroxybutyl)-3-methyl-imidazolium

[HOEMIm]⁺ =

1-(2'-hydroxyethyl)-3-methyl-imidazolium

[HOIm]⁺ =

hydroxy-functionalized imidazolium ILs ,
e. g., 1-(2',3'-dihydroxypropyl)-3-methyl-imidazolium

[HSCO₂Im]⁺ =

1-methyl-3-(2'-mercaptoacetoxyethyl)-imidazolium

[HSIm]⁺ =

X = O(CO)CH₂SH

thiol-functionalized imidazolium ILs,
e. g., 1-(2',3'-dimercaptoacetoxypropyl)-3-methyl-imidazolium

[NCBMIm]⁺ =

1-butyronitrile-3-methyl-imidazolium

[ShexMIm]⁺ =

3.3'-[disulfanylbis(hexane-1,6-diyl)]-bis(1-methyl-imidazolium)

[TriglyMIm]⁺ =

1-triethylene glycol monomethyl ether-3-methyl-imidazolium

[BIMB]²⁺ = 4,4'-bis-[(1,2-dimethylimidazolium)methyl]-2,2'-bipyridine
[BIHB]²⁺ = 4,4'-bis-[7-(2,3-dimethylimidazolium)heptyl]-2,2'-bipyridine
[BIMB][Tf₂N]₂ n = 1
[BIHB][Tf₂N]₂ n = 7

2 Tf₂N⁻

[Gem-IL]²⁺ = gemini / geminal-ILs

OMe

2 Br⁻
5·2Br

2 Br⁻   1·2Br n = 7
2·2Br n = 9
3·2Br n = 15

2 Br⁻
4·2Br

[NCCₙMIm]⁺ =

NC(CH₂)ₙ

1-alkylnitrile-3-methyl-imidazolium
(n = 1-4)

[NCC₃dMIm]⁺ =

NC(CH₂)₃

1-alkylnitrile-2,3-dimethyl-imidazolium

Fig. 12 Examples of functionalized imidazolium ILs. Graphical collection reprinted with permission from the author of Ref. [30]. Copyright Wiley-VCH 2013

A special type of functionalized ILs are gemini imidazolium amphiphiles (cf. Figure 12) [192]. Gemini-type ILs based on imidazolium salts are investigated as simultaneous nanoparticle stabilizers, surfactants and transfer agents into organic media. Au-NPs with imidazolium ligands of the gemini-ILs **1**·2Br to **4**·2Br (cf. Figure 12) that are stable in dispersion and where the IL plays a triple role: phase transfer of the gold precursor salt H[AuCl$_4$] from an aqueous phase to toluene during the synthesis, stabilization of the gold colloid, and binding agent for an ibuprofenate guest. The bis-imidazolium IL ions around the gold nanoparticles do not exchange with thiolate ligands. When both species are present the gold surface prefers the IL cation and anion to thioether ligands. The long alkyl chains in **3**·2Br (cf. Figure 12) could incorporate ibuprofenate, a model for carboxylate-containing anionic drugs, and release it at a slower rate [192].

7 *N*-Heterocyclic Carbene Formation During Metal Nanoparticle Synthesis in Imidazolium ILs

During the last 20 years *N*-heterocyclic carbenes (NHCs) established themselves as a leading class of ligands in molecular organometallic chemistry [193]. NHCs are neutral electron-rich σ-donor ligands, which often form very strong metal ligand σ-bonds. These properties would also be very attractive for the stabilization and reactivity modulation of metal NPs [194–197]. NHCs have been proven to bind efficiently to the surfaces of Ru- [198–201], Ag- [202], Au- [202–205], Pd-[205, 206] and Pt-NPs [207]. Furthermore, there is evidence that NHCs could be intermediate species, by in situ deprotonation of the imidazolium cation at the acidic C2-H position when NPs are formed and stabilized in imidazolium-based ionic liquids for Au-NPs [208], Pd-NPs [208, 209], Rh-NPs [210], Ir-NPs [210, 211] and Ni-NPs [212].

NHC-stabilization of Au- and Pd-NPs was promoted by deprotonation of the bis(*N*,*N'*-*n*-hexyl)imidazolium cation [C$_6$C$_6$Im]$^+$ prior to reduction. This was achieved by treating the imidazolium salt [C$_6$C$_6$Im]$^+$ $_n$[MCl$_4$]$^{n-}$ with sodium
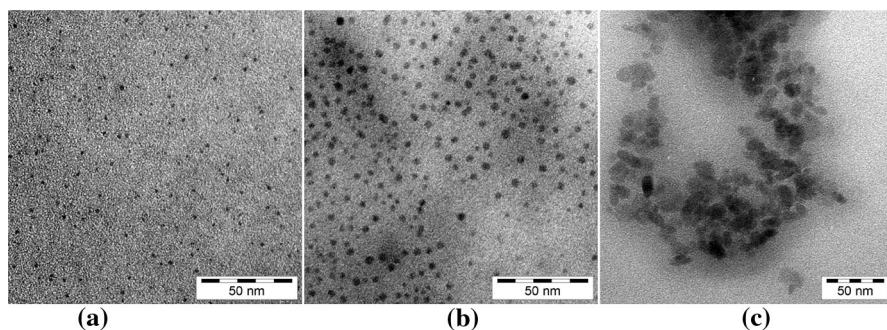
Fig. 13 TEM-images of Co-NPs in [CEMIm or HO$_2$CC$_2$C$_1$Im][BF$_4$] (cf. Figure 12) **a** 6 weeks after synthesis; **b** 6 months after synthesis; **c** Co-NPs from Co$_2$(CO)$_8$ in [BMIm][BF$_4$]. Reprinted with permission. Copyright the Royal Society of Chemistry, 2011 [191]

hydride in 1: 1 dichloromethane–toluene, before adding sodium borohydride to reduce the tetrachloridoaurate(III) ($n = 1$) and dibromidodichloridopalladate(II) ($n = 2$) metal precursor. The ^1H NMR spectrum of the Au-NPs revealed the disappearance of the acidic imidazolium C2 proton resonance, while broadening and splitting was observed for the other peaks, which is typical of NP-coordinated ligands. ^{13}C NMR also failed to locate a peak for C2, which is probably due to anisotropy resulting from the NHC to Au-NP surface coordination. Conversely, the C2 ^1H peak was observed for the Pd-NPs produced without prior imidazolium deprotonation. TEM analysis gave slightly larger sizes of 2.7 ± 0.9 nm for the NHC-capped Pd-NPs than for the imidazolium halide surfactant stabilized Pd-NPs with 1.8 ± 0.4 nm [208].

The Pd-NHC complex $(C_4C_1Im\text{-}NHC)Pd(PPh_3)X$ (X = Br, Cl) formed from $[Pd(Ar)Br(PPh_3)_2]$ and $[PdCl_2(PPh_3)_2]$ in $[C_4C_1Im][BF_4]$ when aqueous Na_2CO_3 was added for imidazolium deprotonation [209].

NHC complexes of rhodium and iridium were obtained in neat $[C_4C_1Im][NTf_2]$ from metal complexes with basic anionic ligands, $[M(COD)(PPh_3)X]$, X = OEt, $MeCO_2$, which reacted with the imidazolium cation under deprotonation giving the M-NHC moiety and the free protonated base HOEt, $MeCO_2H$ [210].

The synthesis of Ir nanoparticles by reduction of $[(COD)Ir(CH_3CN)_2]BF_4$ with H_2 or D_2 in the presence of Proton Sponge (PS^{TM}) in acetone with set but variable amounts of $[C_4C_1Im][NTf_2]$ gave evidence for the formation of at least transiently surface-ligand-coordinated NHCs. When using D_2 deuterium incorporation was apparent from ^2H NMR spectroscopy at the imidazolium C2-H, C4-H, C5-H, and butyl $-(CH_2CH_2)C8\text{-}H(CH_3)$ positions of the $[C_4C_1Im]^+$ cation. Conversely, ^1H NMR spectra showed a decreased intensity of the 2-, 4-, 5-, and 8-H hydrogens in the $[C_4C_1Im]^+$ cation. Without the presence of Ir-NPs no D incorporation into the imidazolium cation occured. A sequence of N-heterocyclic carbene formation by oxidative addition of the imidazolium cation, followed by H/D scrambling atop the nanoparticle surface, then reductive elimination of a imidazolium-C-D bond is suggested [211].

During the auto-decomposition of $Ni(COD)_2$ in imidazolium ILs the formation of bis(imidazolylidene)nickel complexes $[(NHC)_2NiH]^+$ was detected by mass spectrometry [212].

8 Conclusion

In the last years many different M-NPs (monometallic and bimetallic) in ILs were obtained. Especially ILs with imidazolium cations feature prominently in the formation and stabilization of M-NPs. Such imidazolium ILs simultaneously act as reaction media, hydrogen sources, catalysts, templating agents and stabilizers for the synthesis of metal nanoparticles.

Various and also yet unknown factors influence the stability of nanoparticles in ionic liquids and lead to nanoparticle size and/or morphology changes during synthesis. An improved understanding of the stability of nanoparticle dispersions in

ionic liquids is still needed to assist efforts directed toward the synthesis of nanoparticles with controlled size and morphology in ionic liquids.

An influence of the anion to metal nanoparticles was also observed by several other research groups. Qualitatively, the size of M-NPs was found to increase with the molecular volume of the anion of the IL. Also, an influence of the imidazolium alkyl-chain length on the particle size of M-NPs is often invoked, yet the unclear direction. It is both found that the NP size increased with increasing chain lengths whereas in other studies an increase of the alkyl chain gave nanoparticles with a smaller diameter and size-distribution.

It is evident from many reports on cation and anion effects of ILs that the interaction between an IL and a (growing) nanocrystal is far from understood but that a detailed understanding of the IL–nanoparticle interaction would be needed for a more rational design of nanomaterials in ILs.

Furthermore, thiol-, ether-, carboxylic acid-, amino- and hydroxyl-functionalized ILs can be used to coordinate to the surface of metal NPs akin to the action of coordinating capping ligands. Also, for imidazolium-based ionic liquids there is evidence that *N*-heterocyclic carbenes, NHCs could be formed by in situ deprotonation of the imidazolium cation at the acidic C2-H position, at least as intermediate species, during the nanoparticle seeding and growth process.

References

1. Sankar M, Dimitratos N, Miedziak PJ, Wells PP, Kiely CJ, Hutchings GJ (2012) Chem Soc Rev 41:8099–8139
2. Turkevich J, Stevenson PC, Hillier J (1951) Discuss Faraday Soc 11:55–75
3. Brust M, Walker M, Bethell D, Schriffrin DJ, Whyman RJ (1994) J Chem Soc Chem Commun 801–802
4. Bönnemann H, Braun G, Brijoux W, Brinkmann R, Schulze Tilling A, Seevogel K, Siepen K (1996) J Organomet Chem 520:143–162
5. Aiken JD III, Finke RG (1999) J Mol Catal A 145:1–44
6. Schmid G (2001) Nanoscale materials in chemistry In: Klabunde KJ (ed) Wiley-Interscience, New York, p 15
7. Faraday M (1857) Philos Trans R Soc. London 147:145–181
8. Manojkumar K, Sivaramakrishna A, Vijayakrishna K (2016) J Nanopart Res 18:103–125
9. Lu AH, Salabas EL, Schüth F (2007) Angew Chem Int Ed 46:1222–1244
10. Feldheim DL, Foss CA (2001) Metal nanoparticles: synthesis, characterization and applications. Taylor and Francis, London
11. Bruchez M, Moronne M, Gin P, Weiss S, Alivisatos AP (1998) Science 281:2013–2016
12. Saha K, Agasti SS, Kim C, Li X, Rotello VM (2012) Chem Rev 112:2739–2779
13. Li JH, Zhang JZ (2009) Coord Chem Rev 253:3015–3041
14. Barnes WL, Dereux A, Ebbesen TW (2003) Nature 424:824–830
15. Poizot P, Laruelle S, Grugeon S, Dupont L, Tarascon JM (2000) Nature 407:496–499
16. Armelao L, Quici S, Barigelletti F, Accorsi G, Bottaro G, Cavazzini M, Tondello E (2010) Coord Chem Rev 254:487–505
17. Navalon S, Dhakshinamoorthy A, Alvaro M, Garcia H (2016) Coord Chem Rev 312:99–148
18. Walker JM, Zaleski JM (2016) Nanoscale 8:1535–1544
19. Zhao P, Feng X, Huang D, Yang G, Astruc D (2015) Coord Chem Rev 287:114–136
20. Redel E, Thomann R, Janiak C (2008) Inorg Chem 47:14–16

21. Migowski P, Zanchet D, Machado G, Gelesky MA, Teixeira SR, Dupont J (2010) Phys Chem Chem Phys 12:6826–6833
22. Pachon LD, Rothenberg G (2008) Appl Organomet Chem 22:288–299
23. Lee W, Scholz R, Nielsch K, Gösele U (2005) Angew Chem 117:6204–6208
24. Davar F, Loghman-Estarki MR, Salavati-Niasari M, Mazaheri M (2016) J Clust Sci 27:593–603
25. Wang H, Xu JZ, Zhu JJ, Chen HY (2002) J Cryst Growth 244:88–94
26. Chen WX, Lee JY, Liu Z (2002) Chem Commun 2588-2589
27. Sreeju N, Rufus A, Philip D (2016) J Mol Liq 221:1008–1021
28. Qin Y, Ji X, Jing J, Liu H, Wu H, Yang W (2010) Colloids Surf A 372:172–176
29. Goesmann H, Feldmann C (2010) Angew Chem Int Ed 49:1362–1395
30. Janiak C (2013) Z Naturforschung B 68:1059–1089. doi:10.5560/ZNB.2013-3140
31. Hostetler MJ, Wingate JE, Zhong C-J, Harris JE, Vachet RW, Clark MR, Londono JD, Green SJ, Stokes JJ, Wignall GD, Glish GL, Porter MD, Evans ND, Murray RW (1998) Langmuir 14:17–30
32. Templeton AC, Wuelfing WP, Murray RW (2000) Acc Chem Res 33:27–36
33. Weare WW, Reed SM, Warner MG, Hutchison JE (2000) J Am Chem Soc 122:12890–12891
34. Schmid G, Pfeil R, Boese R, Bandermann F, Meyer S, Calis GHM, van der Velden JWA (1981) Chem Ber 114:3634–3642
35. Yang J, Deivaraj TC, Too H-P, Lee JY (2004) Langmuir 20:4241–4245
36. Pan C, Pelzer K, Philippot K, Chaudret B, Dassenoy F, Lecante P, Casanove MJ (2001) J Am Chem Soc 123:7584–7593
37. Lee CL, Wan CC, Wang YY (2001) Adv Funct Mater 11:344–347
38. Tiwari AK, Gangopadhyay S, Chang CH, Pande S, Saha SK (2015) J Colloid Interface Sci 445:76–83
39. Esumi K, Hara J, Aihara N, Usui K, Torigoe K (1998) J Colloid Interface Sci 208:578–581
40. Xu J, Hu J, Peng C, Liu H, Hu Y (2006) J Colloid Interface Sci 298:689–693
41. Bakshi MS, Sharma P, Banipal TS (2007) Mater Lett 61:5004–5009
42. Song C, Wu D, Zhang F, Liu P, Lu Q, Feng X (2012) Chem Commun 48:2119–2121
43. Kumar KS, Vasuki R, Priya R (2016) J Pharm Techn 8:12130–12143
44. Demir MM, Gulgun MA, Menceloglu YZ, Erman B, Abramchuk SS, Makhaeva EE, Khokhlov AR, Matveeva VG, Sulman MG (2004) Macromolecules 37:1787–1792
45. Crespy D, Landfester K (2009) Polymer 50:1616–1620
46. Huang H, Yang X (2004) Carbohydr Res 339:2627–2631
47. Vollmer C, Janiak C (2011) Coord Chem Rev 255:2039–2057
48. Wender H, Migowski P, Feil AF, Teixeira SR, Dupont J (2013) Coord Chem Rev 257:2468–2483
49. Welton T (2004) Coord Chem Rev 248:2459–2477
50. Welton T (1999) Chem Rev 99:2071–2083
51. Hallett JP, Welton TT (2011) Chem Rev 111:3508–3576
52. Morris RE (2009) Chem Commun 2990–2998
53. Voronchikhina LI, Zhuralev OE, Verolainen NV, Krotova NI (2016) Russ J Gen Chem 86:1314–1318
54. Villanueva M, Coronas A, Garcia J, Salgado J (2013) Ind Eng Chem Res 52:15718–15727
55. Kosmulski M, Gustafsson J, Rosenholm JB (2004) Thermochim Acta 412:47–53
56. Ngo HL, LeCompte K, Hargens L, McEwen AB (2000) Thermochim Acta 357–358:97–102
57. Chen G, Kang S, Ma Q, Chen W, Tang Y (2014) Magn Reson Chem 52:673–679
58. Craig SL (2009) Angew Chem Int Ed 48:2645–2647
59. Daniel MC, Astruc D (2004) Chem Rev 104:246–293
60. Parvulescu VI, Hardacre C (2007) Chem Rev 107:2615–2665
61. Steinrück HP, Wasserscheid P (2015) Catal Lett 145:380–397
62. Freudenmann D, Wolf S, Wolff M (2011) Feldmann C. Angew Chem 123:11244–11255
63. Dupont J, de Souza RF, Suarez PAZ (2002) Chem Rev 102:3667–3691
64. Tokuda H, Hayamizu K, Ishii K (2005) Susan MdABH, Watanabe M. J Phys Chem B 109:6103–6110
65. Dupont J, Scholten JD (2010) Chem Soc Rev 39:1780–1804
66. Marcos Esteban R, Janiak C (2017) In Nanocatalysis in Ionic Liquids In: Prechtl M (ed) chapter 8. Wiley-VCH, Weinheim, p 147–169
67. Janiak C (2014) in Catalysis in ionic liquids: from catalyst synthesis to application In: Hardacre C, Parvulescu V, chapter 11. RSC Publishing, Cambridge, p 537–577
68. Janiak C (2015) Topics Organomet Chem 51:17–53. doi:10.1007/3418_2013_70

69. Antonietti M, Kuang D, Smarsly B, Zhou Y (2004) Angew Chem Int Ed 43:4988–4992
70. Fonseca GS, Umpierre AP, Fichtner PFP, Teixeira SR, Dupont J (2003) Chem Eur J 9:3263–3269
71. Huang J, Jiang T, Han B, Gao H, Chang Y, Zhao G, Wu W (2003) Chem Commun 1654-1655
72. Krämer J, Redel E, Thomann R, Janiak C (2008) Organometallics 27:1976–1978
73. Silveira ET, Umpierre AP, Rossi LM, Machado G, Morais J, Soares GV, Baumvol IJR, Teixeira SR, Fichtner PFP, Dupont J (2004) Chem Eur J 10:3734–3740
74. Redel E, Walter M, Thomann R, Hussein L, Krüger M, Janiak C (2010) Chem Commun 46:1159–1161
75. Stellaci F, Bauer CA, Meyer-Friedrichsen T, Wenseleers W, Alain V, Kuebler SM, Pond SJK, Zhang Y, Marder SR, Perry JW (2002) Adv Mater 14:194–198
76. Mohan B, Woo H, Jang S, Lee S, Park S, Park KH (2013) Solid State Sci 22:16–20
77. Zhang B, Yuan Y, Philippot K, Yan N (2015) Catal Sci Technol 5:1683–1692
78. Khare V, Li Z, Mantion A, Ayi AA, Sonkaria S, Voelkl A, Thünemann AF, Taubert A (2010) J Mater Chem 20:1332–1339
79. Jiang HY, Zheng HH (2015) Appl Cat A 499:118–123
80. Dewan M, De A (2015) Mozumdar. Inorg Chem Commun 53:92–96
81. Esteban RM, Meyer H, Kim J, Gemel C, Fischer RA, Janiak C (2016) Eur J Inorg Chem 2106-2113
82. Schütte K, Meyer H, Gemel C, Barthel J, Fischer RA, Janiak C (2014) Nanoscale 6:3116–3126
83. Esteban RM, Schütte K, Brandt P, Marquardt D, Meyer H, Beckert F, Mülhaupt R, Kölling H, Janiak C (2015) Nano-Struct Nano-Objects 2:11–18
84. Ayi AA, Anyama CA, Khare V (2015) J Mat, vol. 2015, Article ID 372716, http://dx.doi.org/10.1155/2015/372716
85. Andanson JM, Marx S, Baiker A (2012) Catal Sci Technol 2:1403–1409
86. Schütte K, Doddi A, Kroll C, Meyer H, Wiktor C, Gemel C, van Tendeloo G, Fischer RA, Janiak C (2014) Nanoscale 6:5532–5544
87. Wegner S, Saito M, Barthel J, Janiak C (2016) J Organomet Chem 821:192–196
88. Wang Y, Yang H (2005) J Am Chem Soc 127:5316–5317
89. Arquillière PP, Helgadottir IS, Santini CC, Haumesser P-H, Aouine M, Massin L, Rousset J-L (2013) Top Catal 56:1192–1198
90. Dash P, Dehm NA, Scott RWJ (2008) J Mol Catal A 286:114–119
91. Stankus DP, Lohse SE, Hutchison JE, Nason JA (2010) Environ Sci Technol 45:3238–3244
92. Astruc D (2008) Nanoparticles and catalysis. Wiley Online Library, Weinheim
93. Jiang J, Oberdörster G, Biswas P (2009) J Nanopart Res 11:77–89
94. Kim T, Lee K, Gong M-s, Joo S-W (2005) Langmuir 21:9524–9528
95. Derjaguin B, Landau L (1940) Acta Phys Chem USSR 14:1–30
96. Verwey EJW, Overbeek JThG (1948) Theory of the stability of lyophobic colloids. Elsevier, Amsterdam
97. Li Q, Jonas U, Zhao XS, Kappl M (2008) Asia-Pac J Chem Eng 3:255–268. doi:10.1002/apj.144
98. Ninham BW (1999) Adv Col Interf Sci 83:1–17
99. Raveendran P, Fu J, Wallen SL (2003) J Am Chem Soc 125:13940–13941
100. Verwey EJW, Overbeek JTG (1999) Theory of the stability of lyophobic colloids. Dover Publications Mineola, New York
101. Finke RG (2002) Metal nanoparticle: synthesis, characterization and applications. Marcel Dekker, New York
102. Ott LS, Finke RG (2006) Inorg Chem 45:8283–8393
103. Boström M, Williams DRW, Ninham BW (2001) Phys Rev Lett 87:168103–168107
104. Liang Y, Hilal N, Langston P, Starov V (2007) Adv Col Interf Sci 134–135:151–166
105. Sarkar B, Venugopal V, Tsianou M, Alexandridis P (2013) Col Surf 422:155–164
106. Napper DH (1977) J Col Interf Sci 58:390–407
107. Lin Y, Smith TW, Alexandridis P (2002) J Col Interf Sci 255:1–9
108. Luckham PF (1991) Adv Col Interf Sci 34:191–215
109. Morrison ID, Ross S (2002) Colloidal dispersions: suspensions, emulsions, and foams. Wiley-Interscience, New York
110. Zhao M, Li N, Zheng L, Li G, Yu L (2008) J Dispers Sci Technol 29:1103–1105
111. Obliosca JM, Arellano IHJ, Huang MH, Arco SD (2010) Mater Lett 64:1109–1112
112. Rubim JC, Trindade FA, Gelesky MA, Aroca RF, Dupont J (2008) J Phys Chem C 112:19670–19675

113. Schrekker HS, Gelesky MA, Stracke MP, Schrekker CML, Machado G, Teixeira SR, Rubim JC, Dupont J (2007) J Col Interf Sci 316:189–195
114. Chun YS, Shin JY, Song CE, Lee SG (2008) Chem Commun 942–944
115. Zhang H, Cui H (2009) Langmuir 25:2604–2612
116. Scheeren CW, Machado G, Teixeira SR, Morais J, Domingos JB, Dupont J (2006) J Phys Chem B 110:13011–13020
117. Fonseca GS, Machado G, Teixeira SR, Fecher GH, Morais J, Alves MCM, Dupont J (2006) J Col Interf Sci 301:193–204
118. Kang SW, Char K, Kang YS (2008) Chem Mater 20:1308–1311
119. Redel E, Walter M, Thomann R, Vollmer C, Hussein L, Scherer H, Krüger M, Janiak C (2009) Chem Eur J 15:10047–10059
120. Pearson RG (1997) Chemical hardness. Application from molecules to solids. Wiley-VCH, Weinheim
121. Baker TA, Friend CM, Kaxiras E (2008) J Am Chem Soc 130:3720–3721
122. Katsyuba SA, Zvereva EE, Yan N, Yuan X, Kou Y, Dyson PJ (2012) ChemPhysChem 13:1781–1790
123. Kim J, Kang SW, Mun SH, Kang YS (2009) Ind Eng Chem Res 48:7437–7441
124. Yuan X, Yan N, Katsyuba SA, Zvereva EE, Kou Y, Dyson PJ (2012) Phys Chem Chem Phys 14:6026–6033
125. He Z, Alexandridis P (2015) Phys Chem Chem Phys 17:18238–18261
126. Kang X, Sun X, Han B (2016) Adv Mater 28:1011–1030
127. Vanecht E, Binnemans K, Patskovsky S, Meunier M, Seo JW, Stappers L, Fransaer J (2012) Phys Chem Chem Phys 14:5662–5671
128. Podgorsek A, Pensado A, Santini C, Gomes M, Padua A (2013) J Phys Chem C 117:3537–3547
129. Frolov AI, Kirchner K, Kirchner T, Fedorov MV (2012) Faraday Discuss 154:235–247
130. Cheng P, Liu C, Yang Y, Huang S (2015) Chem Phys 452:1–8
131. Pensado AS, Padua AAH (2011) Angew Chem 123:8842–8846
132. Knapp R, Wyrzgol SA, Reichelt M, Hammer T, Morgner H, Müller TE, Lercher JA (2010) J Phys Chem C 114:13722–13729
133. Bernardi F, Scholten JD, Fecher GH, Dupont J, Morais J (2009) Chem Phys Lett 479:113–116
134. Rosen MJ, Kunjappu JT (2012) Surfactants and Interfacial Phenomena. Wiley, Weinheim
135. Li Q, Li A (2012) Asian J Chem 24:847–850
136. Wender H, de Oliveira LF, Migowski P, Feil AF, Lissner E, Prechtl MHG, Teixeira SR, Dupont J (2010) J Phys Chem C 114:11764–11768
137. Torimoto T, Okazaki KI, Kiyama T, Hirahara K, Tanaka N, Kuwabata S (2006) Appl Phys Lett 89:243117
138. Hatakeyama Y, Okamoto M, Torimoto T, Kuwabata S, Nishikawa K (2009) J Phys Chem C 113:3917–3922
139. Kessler MT, Hentschel MK, Heinrichs C, Roitsch S, Prechtl MHG (2014) RSC Adv 4:14149–14156
140. Scariot M, Silva DO, Scholten JD, Machado G, Teixeira SR, Novak MA, Ebeling G, Dupont J (2008) Angew Chem Int Ed 47:9075–9078
141. Wang L, Chang L, Zhao B, Yuan Z, Shao G, Zheng W (2008) Inorg Chem 47:1443–1452
142. Li X, Liu Y, Guo W, Chen J, He W, Peng F (2014) Electrochim Acta 135:550–557
143. Lorbeer C, Cybinska J, Mudring AV (2014) J Mater Chem C 2:1862–1868
144. Patil AB, Bhanage BM (2014) Phys Chem Chem Phys 16:3027–3035
145. Liu CH, Mao BH, Gao J, Zhang S, Gao X, Liu Z, Lee ST, Sun XH, Wang SD (2012) Carbon 50:3008–3014
146. Hatakeyama Y, Takahashi S, Nishikawa K (2010) J Phys Chem C 114:11098–11102
147. Kameyama T, Ohno Y, Kurimoto T, Okazaki KI, Uematsu T, Kuwabata S, Torimoto T (2010) Phys Chem Chem Phys 12:1804–1811
148. Tsuzuki S, Tokuda H, Hayamizu K, Watanabe M (2005) J Phys Chem B 109:16474–16481
149. Hardacre C, Holbrey JD, McMath SEJ, Bowron DT, Soper AK (2003) J Chem Phys 118:273–278
150. Dupont J, Suarez PAZ (2006) Phys Chem Chem Phys 8:2441–2452
151. Gozzo FC, Santos LS, Augusti R, Consorti CS, Dupont J, Eberlin MN (2004) Chem Eur J 10:6187–6193
152. Neto BAD, Santos LS, Nachtigall FM, Eberlin MN, Dupont J (2006) Angew Chem 118:7409–7412
153. Dupont J (2011) Acc Chem Res 44:1223–1231
154. Dong K, Zhang SJ (2012) Chem Eur J 18:2748–2761

155. Chang HC, Hung TC, Chang SC, Jiang JC, Lin SH (2011) J Phys Chem C 115:11962–11967
156. Richter K, Birkner A, Mudring AV (2011) Phys Chem Chem Phys 13:7105–7110
157. Wittmar A, Ulbricht M (2012) Ind Eng Chem Res 51:8425–8433
158. Dupont J (2004) J Braz Chem Soc 15:341–350
159. Schröder U, Wadhawan JD, Compton RG, Marken F, Suarez PAZ, Consorti CS, de Souza RF, Dupont J (2000) New J Chem 24:1009–1015
160. Tokuda H, Hayamizu K, Ishii K, Hasan Susan MdAB, Watanabe M (2004) J Phys Chem B 108:16593–16600
161. Anderson JL, Armstrong DW (2003) Anal Chem 75:4851–4858
162. Lopes JNA, Padua AAH (2006) J Phys Chem B 110:3330–3335
163. Reddy RG (2006) J Phase Equilib Diffus 27:210–211
164. Redel E, Krämer J, Thomann R, Janiak C (2009) J Organomet Chem 694:1069–1075
165. Redel E, Thomann R, Janiak C (2008) Chem Commun 15:1789–1791
166. Neouze MA (2010) J Mater Chem 20:9593–9607
167. Peng H, Lin L, Ding G (2015) Energy 89:410–420
168. Navolotskaya DV, Toh HS, Batchelor-McAuley C, Compton RG (2015) ChemistryOpen 4:595–599
169. Wang XM, Zhou DD, Zou QQ, Xia YY (2012) J Mater Chem 22:15418–15426
170. Keul HA, Ryu HJ, Möller M, Bockstaller MR (2011) Phys Chem Chem Phys 13:13572–13578
171. Hong GH, Kang SW (2013) Ind Eng Chem Res 52:794–797
172. Han KI, Kang SW, Kim J, Kang YS (2011) J Membr Sci 374:43–48
173. Lancaster NL, Welton T (2004) J Org Chem 69:5986–5992
174. Yang M, Campbell PS, Santini CC, Mudring AV (2014) Nanoscale 6:3367–3375
175. Gutel T, Santini CC, Philippot K, Padua A, Pelzer K, Chaudret B, Chauvin Y, Basset JM (2009) J Mater Chem 19:3624–3631
176. Banerjee A, Theron R, Scott RWJ (2012) ChemSusChem 5:109–116
177. Jacquemin J, Husson P, Majer V, Costa Gomes MF (2007) J Solut Chem 36:967–979
178. Hatakeyama Y, Okamoto M, Torimoto T, Kuwabata S, Nishikawa K (2009) J Phys Chem C 113:3917–3922
179. Hatakeyama Y, Onishi K, Nishikawa K (2011) RSC Adv 1:1815–1821
180. Migowski P, Machado G, Texeira SR, Alves MCM, Morais J, Traverse A, Dupont J (2007) Phys Chem Chem Phys 9:4814–4821
181. Wegner S, Rutz C, Schütte K, Barthel J, Bushmelev A, Schmidt A, Dilchert K, Fischer RA, Janiak C (2017) Chem Eur J 23:6330–6340 (http://dx.doi.org/10.1002/chem.201605251)
182. Wittmar A, Gajda M, Gautam D, Dörfler U, Winterer M, Ulbricht M (2013) J Nanopart Res 15:1–12
183. Dzyuba S, Bartsch RA (2002) ChemPhysChem 2:161–166
184. Itoh H, Naka K, Chujo Y (2004) J Am Chem Soc 126:3026–3027
185. Chen H, Dong S (2007) Langmuir 23:12503–12507
186. Wei GT, Yang Z, Lee CY, Yang HY, Wang CRC (2004) J Am Chem Soc 126:5036–5037
187. Lewis LN (1993) Chem Rev 93:2693–2730
188. Kim KS, Demberelnyamba D, Lee H (2004) Langmuir 20:556–560
189. Gao S, Zhang H, Wang X, Mai W, Peng C, Ge L (2005) Nanotechnology 16:1234–1237
190. Marcilla R, Mecerreyes D, Odriozola I, Pomposo JA, Rodriguez J (2007) NANO Br Rep Rev 2:169–173
191. Marquardt D, Xie Z, Taubert A, Thomann R, Janiak C (2011) Dalton Trans 40:8290–8293
192. Casal-Dujat L, Rodrigues M, Yagüe A, Calpena AC, Amabilino DB, Gonzalez-Linares J, Borras M, Perez-Garcia L (2012) Langmuir 28:2368–2381
193. Diez-Gonzalez S, Marion N, Nolan SP (2009) Chem Rev 109:3612–3676
194. Richter C, Schaepe K, Glorius F, Ravoo BJ (2014) Chem Commun 50:3204–3207
195. Magna L, Chauvin Y, Niccolai GP, Basset JM (2003) Organometallics 22:4418–4425
196. Lecocq V, Olivier-Bourbigou H (2007) Oil Gas Sci Technol 62:761–773
197. Holloczki O, Gerhard D, Massone K, Szarvas L, Nemeth B, Veszpremi T, Nyulaszi L (2010) New J Chem 34:3004–3009
198. Martinez-Prieto LM, Ferry A, Lara P, Richter C, Philippot K, Glorius F, Chaudret B (2015) Chem Eur J 21:17495–17502
199. Martinez-Prieto LM, Urbaneja CC, Palma P, Campora J, Philippot K, Chaudret B (2015) Chem Commun 51:4647–4650
200. Lara P, Rivada-Wheelaghan O, Conejero S, Poteau R, Philippot K, Chaudret B (2011) Angew Chem Int Ed 50:12286–12290

201. Gonzalez-Galvez D, Lara P, Rivada-Wheelaghan O, Conejero S, Chaudret B, Philippot K, van Leeuwen PWNM (2013) Catal Sci Technol 3:99–105
202. Ling X, Schaeffer N, Roland S, Pileni M (2013) Langmuir 29:12647–12656
203. Roland S, Ling X, Pileni MP (2016) Langmuir 32:7683–7696
204. Vignolle J, Tilley TD (2009) Chem Commun 7230–7232
205. Hurst EC, Wilson K, Fairlamb IJS, Chechik V (2009) New J Chem 33:1837–1840
206. Rühling A, Schaepe K, Rakers L, Vonhören B, Tegeder P, Ravoo BJ, Glorius F (2016) Angew Chem Int Ed 55:5856–5860
207. Baquero EA, Tricard S, Flores JC, de Jesus E, Chaudret B (2014) Angew Chem Int Ed 53:1–6
208. Serpell CJ, Cookson J, Thompson AL, Brown CM, Beer PD (2013) Dalton Trans 42:1385–1393
209. Mathews CJ, Smith PJ, Welton T, White AJP, Williams DJ (2001) Organometallics 20:3848
210. Hintermair U, Gutel T, Slawin AMZ, Cole-Hamilton DJ, Santini CC, Chauvin Y (2008) J Organomet Chem 693:2407–2414
211. Ott LS, Cline ML, Deetlefs M, Seddon KR, Finke RG (2005) J Am Chem Soc 127:5758–5759
212. Prechtl MHG, Campbell PS, Scholten JD, Fraser GB, Machado G, Santini CC, Dupont J, Chauvin Y (2010) Nanoscale 2:2601–2606